Matching the lattice modules of the "ecentral" beam line for a new design of ILC RTML.

Valery Kapin, Nikolay Solyak, Yuri Alexahin

FERMILAB, BATAVIA, IL

January, 2011

1. Introduction

The International Linear Collider (ILC) is a 200-500 GeV center-of-mass high-luminosity linear electron-positron collider. Its 2007 reference design described in the RDR-2007[1] is under modifications now. In this report, a new design of ILC Ring to Main Linac (RTML) is considered. The ILC RTML is the collection of beamlines which transfer the beam from the damping ring (DR) to the main linac on each side of the collider. General requirements for a new structure of RTML are outlined in the report[2].

In this report, an initial part of RTML beginning from DR exit is considered. This part of RTML transporting electron beam ("e") is located in the central area of the ILC ("central"). It is called as the "ecentral" beam line. The basic lattice modules forming the "ecentral" beam-line have been borrowed from the 2007 design and arranged by A. Latina[3] to ensure matching to a new RTML geometry. However, Twiss parameters of lattice modules were not matched yet. This initial design has been implemented as MAD-8 file.

In this report, the matching of Twiss parameters between lattice modules of the "ecentral" beam line is presented. Basically, the matching is performed using quadrupole doublets. Parameters of doublets are firstly approximated with analytical solutions, then they are refined with numerical matching commands of the MAD-8 code. As result, five matching sections have been inserted between lattice modules of the initial "ecentral"

[1] "INTERNATIONAL LINEARCOLLIDER REFERENCE DESIGN REPORT", August, 2007.

[2] N. Solyak, A. Latina (FNAL), "RTML Description (DRAFT)", July 29, 2009

[3] A. Latina, archive file "RTML_Central_Lattice.tgz", 2-Nov-2010.

design. These sections are hereafter called as MATCH1, MATCH2, MATCH2a, MATCH3, MATCH4.

1. Structure of the "ecentral"RTML and global coordinates

As proposed by Susanna Guiducci in September 2010, the connection between DR and RTML should be relocated and set at the exit of the extraction septa. That is, the part of the extraction line, which ensured the compensation of the septa dispersion in the previous design, must be added at the beginning of the RTML. Let's call this part as "DR-exit".

According to the mad8 output table attached to Susanna's e-mail as the file "DSB3.lattice_EXT_sepON.txt", RTML should start after the 7m-drift "DINJ8" from the last septum "PEXT1". The last 3 lines of the table are presented below.

Table 1. Parameters of the end cells of DR.

KEYWORD	NAME	L	S	BETX	ALFX	DX	DPX	BETY	ALFY	X, mm	PX, mrad
"HKICKER"	"PEXT1"	1.0	80.90	72.8600	-0.171613E-01	-0.125726	0.202347E-02	6.44405	-0.201883	130.607	54.0209
"DRIFT"	"DINJ8"	7.0	87.90	73.7730	-0.113264	-0.489708	0.202347E-02	17.1842	-1.33243	508.754	54.0209
"LINE"	"EXT_RTML"	0.0	87.90	73.7730	-0.113264	-0.489708	0.202347E-02	17.1842	-1.33243	508.754	54.0209

As suggested is the Susanna's e-mail, "the s coordinate is zero at the center of the DR straight section". Thus, in the global coordinate with the origin set at the center of the DR straight section, the beginning of the RTML named as "DR-exit" is started in the DR plane at the point $\{X, Y, Z\}=\{0.508754; 0; 87.9\}$, while "DR-exit" starts at the angle $\Theta=0.054$ rad in the MAD conventions. Values of Twiss parameters at the start of the "DRexit" line are shown in the last row of the Table 1.

The general structure of the "ecentral" line is presented in Table 2. Global coordinates at the section boundaries are presented in Table 3. Note that at the end of MATCH1 the beam line is exactly parallel to the straight section of DR (Theta=0). Then it is bent due to vertical and horizontal doglegs. The beam line becomes to be parallel to the DR again at the beginning of MATCH4. Fig. 1 and Fig. 2 show the locations of the section boundaries for horizontal and vertical planes, respectively.

The detailed view of the sections in the neighborhood of the horizontal and vertical doglegs is shown in Fig.3 and Fig.4, respectively. Fig. 5 with detailed view of the first arc of the horizontal dogleg allows us to evaluate the horizontal bend radius as about 38 m. The

Twiss parameters vs. the beam line length for the matched “ecentral” beam-line are presented in Fig.6.

Table.2 sections of the “ecentral” line

Section name or functions	Names of composing sub-LINEs in MAD8 file
MATCH1 including DRexit	DRexit_line_1; DRexit_line_2; oppos_line
first arc of the horizontal dogleg	TURNMATCHR; TURNCELLR; TURNSUPPR;
MATCH2	
EXTRACTION	
MATCH2a	
VDOG	VDOG(vertical dogleg) ; 7cells of VDOGFODO
MATCH3	
second arc of the horizontal dogleg	TURNMATCH; TURNCELL; TURNSUPP
MATCH4	
Match to skew section	cells from the old design (“egetaway”)
Skew correction section	-//-
Match to DR stretch including 4-bend chicane	-//-
DR stretch including post-DR collimation	-//-

Table 3. The global coordinates of the section boundary markers.

No.	elem_label	type	X	Y	Z	sumL	Theta	Phi	Psi
1	BEGINECENTRAL	MARK	0.5088E+00	0.0000E+00	0.8970E+02	0.0000E+00	0.5400E-01	0.0000E+00	0.0000E+00
2	END_MATCH1	MARK	0.2028E+01	0.0000E+00	0.1161E+03	0.2644E+02	-0.2082E-16	0.0000E+00	0.0000E+00
3	BEGIN_MATCH2	MARK	0.1138E+02	0.0000E+00	0.1437E+03	0.5624E+02	0.6538E+00	0.0000E+00	0.0000E+00
4	END_MATCH2	MARK	0.1735E+02	0.0000E+00	0.1514E+03	0.6606E+02	0.6538E+00	0.0000E+00	0.0000E+00
5	BEGIN_MATCH2A	MARK	0.2459E+02	0.0000E+00	0.1609E+03	0.7796E+02	0.6538E+00	0.0000E+00	0.0000E+00
6	END_MATCH2A	MARK	0.2848E+02	0.0000E+00	0.1660E+03	0.8435E+02	0.6538E+00	0.0000E+00	0.0000E+00
7	VDOG_END	MARK	0.5751E+02	0.2143E+01	0.2039E+03	0.1321E+03	0.6538E+00	0.1041E-16	-0.4348E-29
8	BEGIN_MATCH3	MARK	0.8306E+02	0.2143E+01	0.2372E+03	0.1741E+03	0.6538E+00	0.1041E-16	-0.4348E-29
9	END_MATCH3	MARK	0.8491E+02	0.2143E+01	0.2396E+03	0.1772E+03	0.6538E+00	0.1041E-16	-0.4348E-29
10	BEGIN_MATCH4	MARK	0.9425E+02	0.2143E+01	0.2674E+03	0.2072E+03	0.6245E-16	0.8262E-17	0.6331E-17
11	END_MATCH4	MARK	0.9425E+02	0.2143E+01	0.2708E+03	0.2106E+03	0.6245E-16	0.8262E-17	0.6331E-17
12	MRK4	MARK	0.9425E+02	0.2143E+01	0.2784E+03	0.2182E+03	0.6245E-16	0.8262E-17	0.6331E-17
13	MRK5	MARK	0.9425E+02	0.2143E+01	0.3395E+03	0.2793E+03	0.6245E-16	0.8262E-17	0.6331E-17
14	MRK6	MARK	0.9425E+02	0.2143E+01	0.3639E+03	0.3037E+03	0.6592E-16	0.8262E-17	0.6331E-17
15	ENDECENTRAL	MARK	0.9425E+02	0.2143E+01	0.1289E+04	0.1229E+04	0.6592E-16	0.8262E-17	0.6331E-17

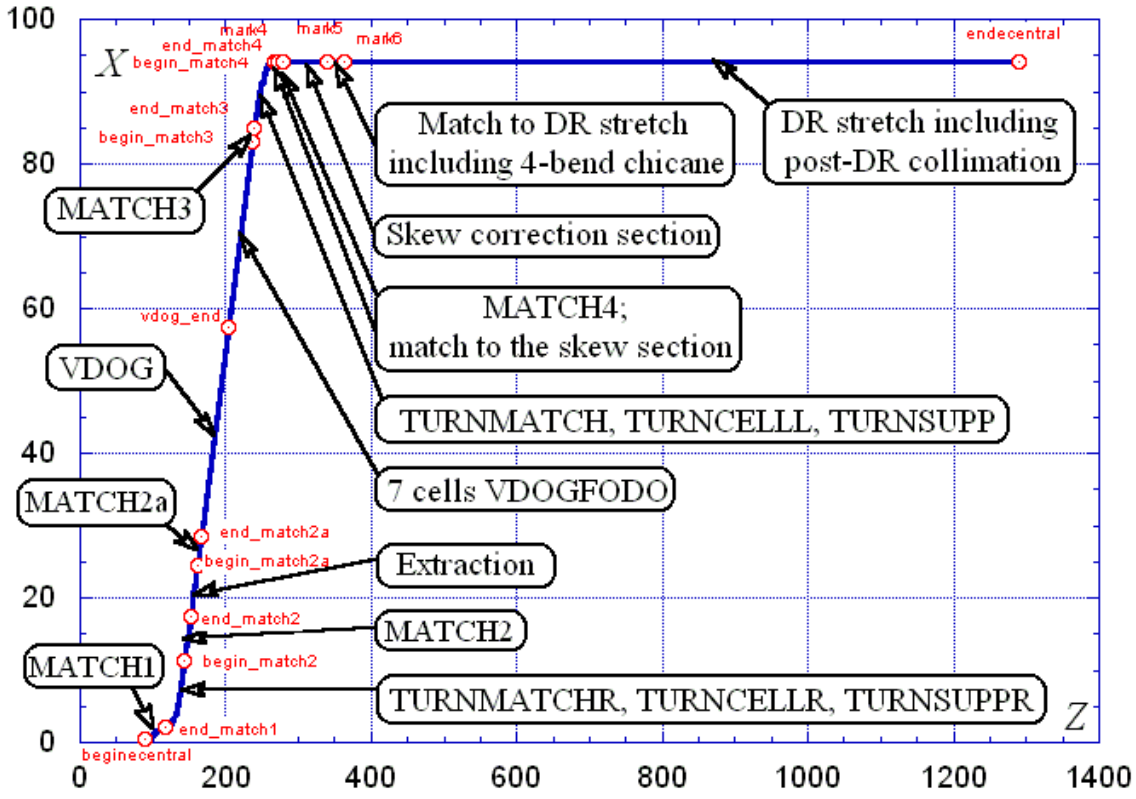

Fig.1 The horizontal projection of the "ecentral" in the global coordinates *X* and *Z*.

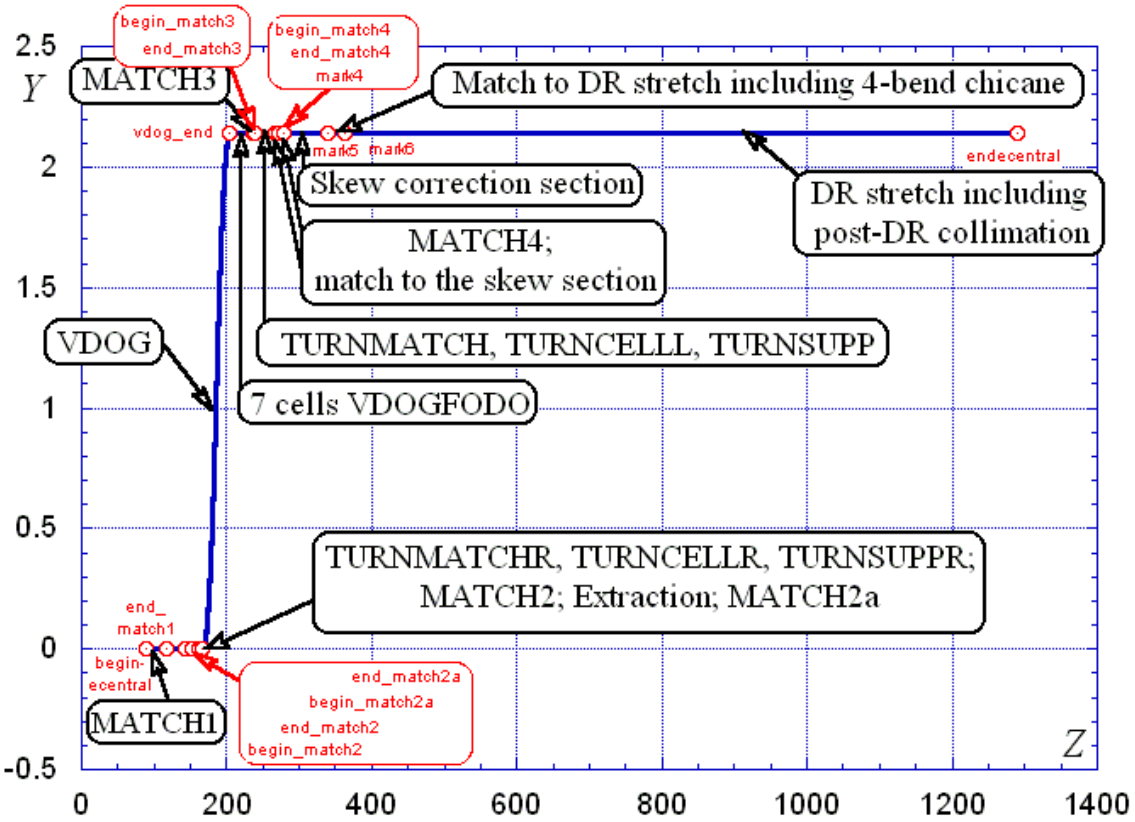

Fig.2 The vertical projection of the "ecentral" in the global coordinates *Y* and *Z*.

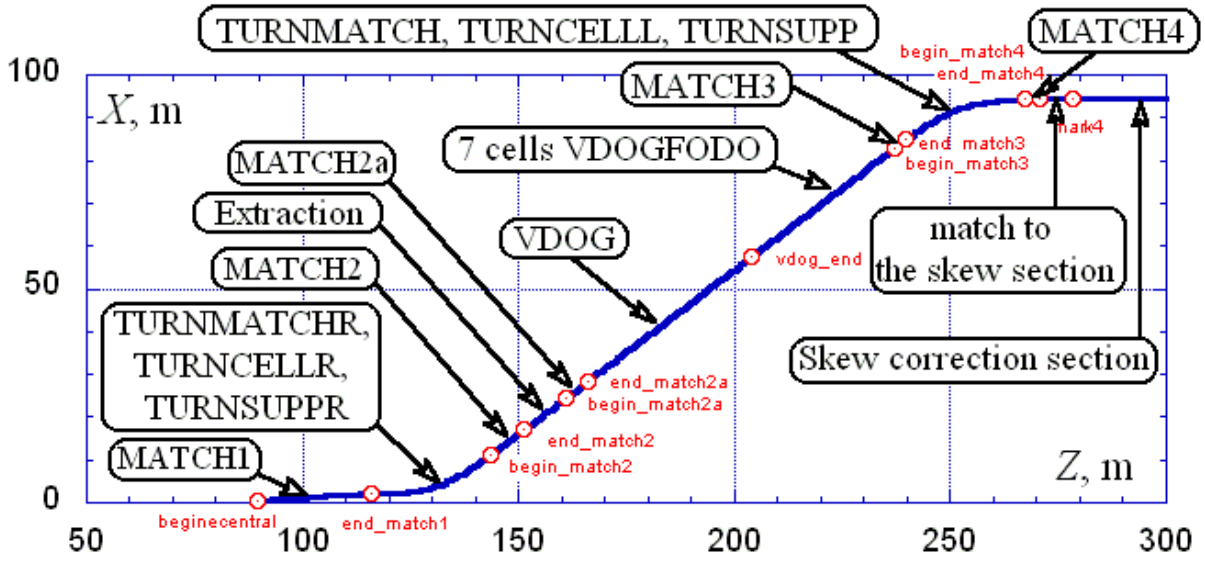

Fig.3 The horizontal projection of the horizontal dogleg in the global coordinates.

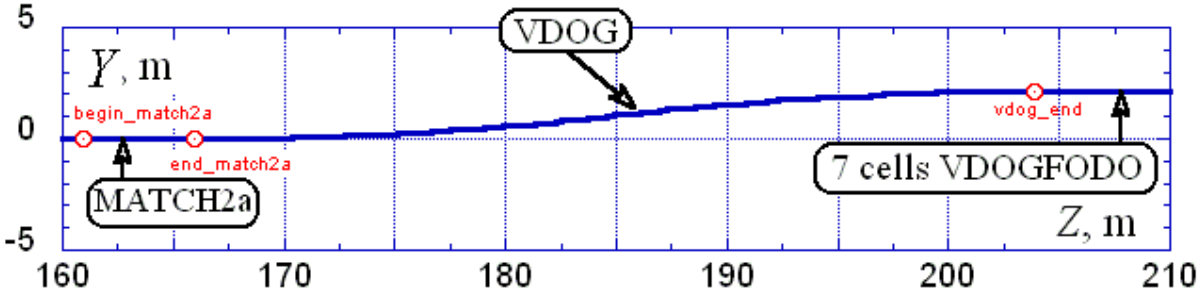

Fig.4 The vertical projection of the vertical dogleg in the global coordinates.

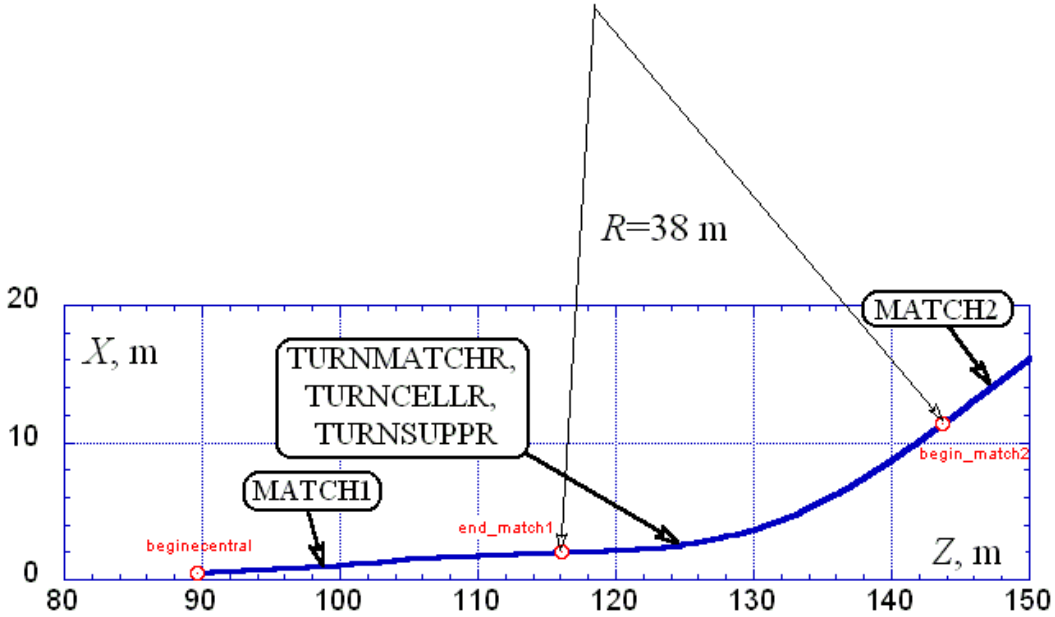

Fig. 5 with detailed view of the first arc of the horizontal dogleg.

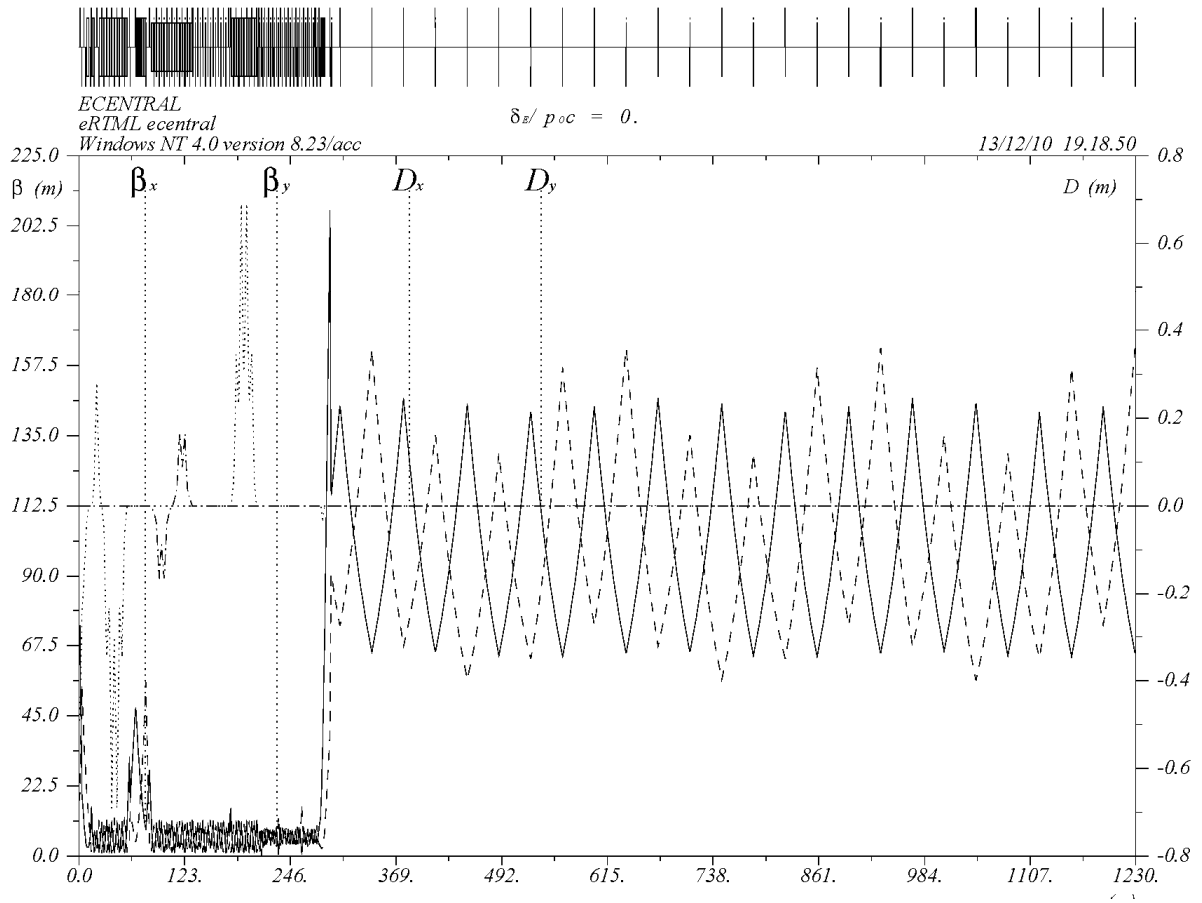

Fig. 6. The Twiss parameters $\beta_{x,y}$ and the dispersion $D_{x,y}$ along the "ecentral" line.

MATCH1 section

The MATCH1 section consists of three logical sections named as "DRexit_line_1", "DRexit_line_2", and "Oppos_line". Note, that "DRexit" formed by two first sections is a part of MATCH1. Values of Twiss parameters at boundaries of the MATCH1 lines are show in the table below.

Table 4. Twiss parameters in the sections of the MATCH1.

Name of line	β_x	α_x	β_y	α_y	D_x	D'_x
start of ERTML	73.773	-0.0171	17.184	-1.332	-0.490	0.002
end of "DRexit_line_1"	6.028	-1.183	6.364	+1.087	0	0
end of "DRexit_line_2"	10.835	3.023	1.157	-0.290	0	0
end of "Oppos_line"	10.835	3.023	1.157	-0.290	0	0

The “DRexit_line_1” consists of 4 quadrupoles ending with bending magnet. This line should ensure zero dispersion and its derivative at the end. The “DRexit_line_2” is quadrupole doublet, which match $\beta_{x,y}$ and $\alpha_{x,y}$ values to the values given at the end of DRexit. The “Oppos_line” consists of the symmetrical quadrupole triplet with two bends and a final quadrupole. It provides an opposite bend returning the beam line to be a parallel with DR straight section, while it translates $\beta_{x,y}$ and $\alpha_{x,y}$ values from the entrance to the exit. In the presented design of the “DRexit” line the same magnets as in old Ina Reichel’s design of the DR extraction are used, namely the 0.3 m quadrupole “Q60L300V4” and 2.0 m dipole “D60L2000” magnets. Dependence of the Twiss parameters along the beam line is shown in Figure 7.

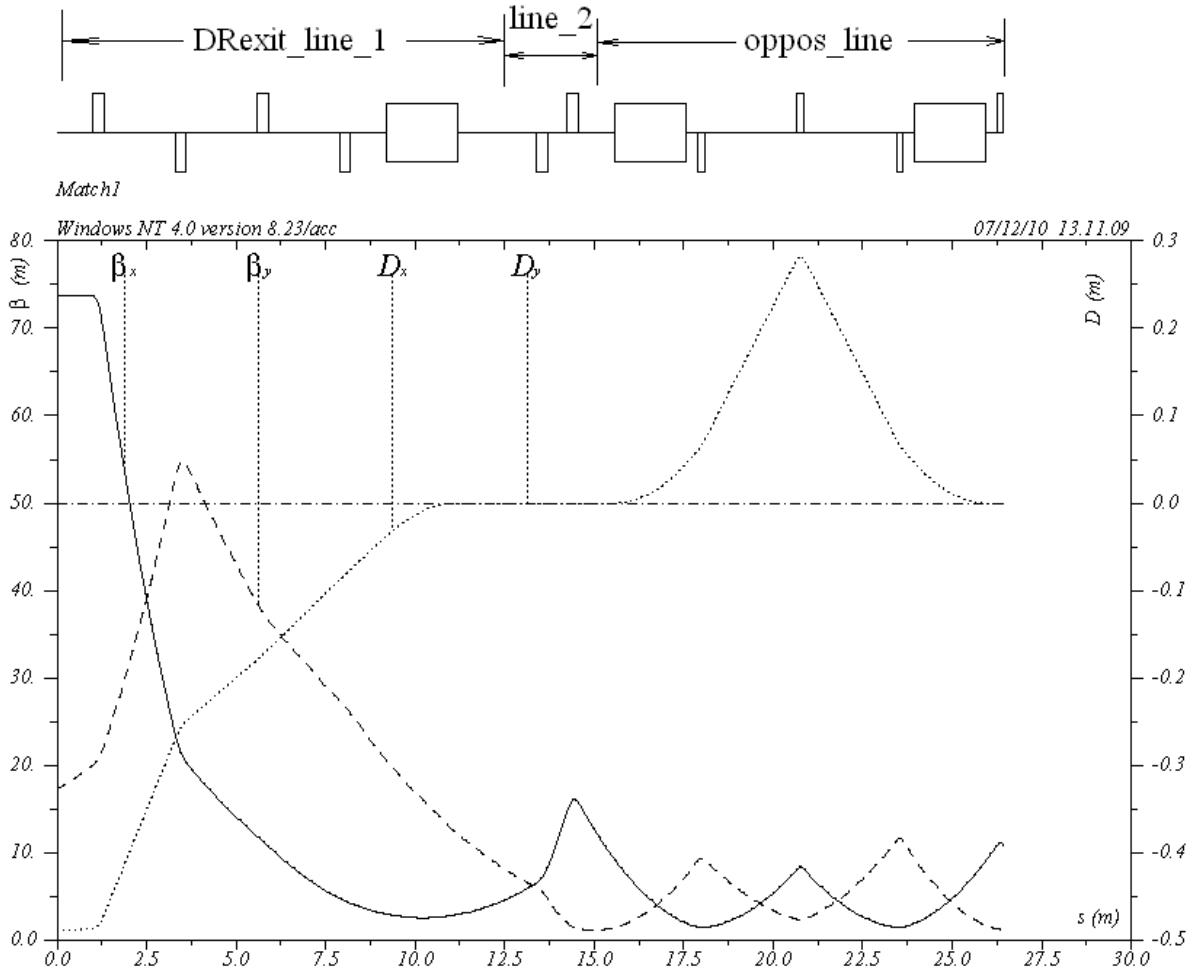

Fig. 7. The Twiss parameters $\beta_{x,y}$ and the dispersion $D_{x,y}$ along MATCH1 section.

Figure 8,a shows the projection of the “DRexit” beam line in the horizontal plane of

the global coordinates X and Z, and the cumulative length "sumL" as a function of Z-coordinate. To illustrate the direction of the "DRexit" line in the horizontal $\{X,0,Z\}$-plane, Figure 8,b presents the dependence of the angle "Theta" (rotation about the vertical Y-axis) on the Z-coordinate. The initial rotation of Θ =0.054 rad is increased to Θ=0.108 rad after the first dipole located the exit of "DRexit_line_1". Then, two dipoles of the "Oppos_line" bring the Θ-value to zero, and the end of the "DRexit" line becomes parallel to the DR straight section.

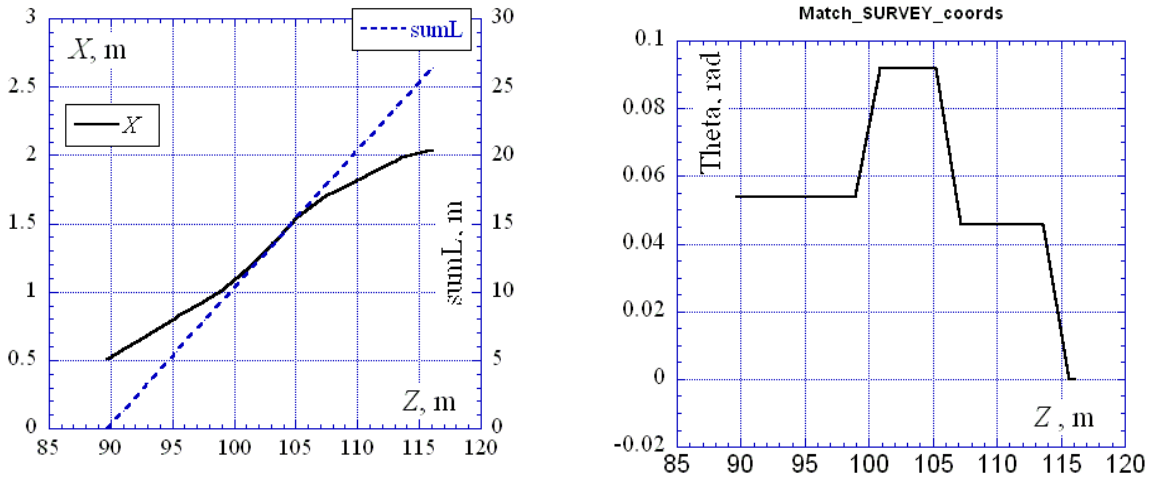

a) Y vs. Z. b) Θ vs. Z.

Fig. 8. The reference trajectory of the "DRexit" line.

The matching of the "DRexit_line_1" and "Oppos_line" have been performed purely numerically with minimization algorithms using MAD matching commands. The details of the matching for "DRexit_line_2" consisting of quadrupole doublet (Q2) is presented below.

Matching with quadrupole doublet

The quadrupole doublet performs the transformation of the Twiss parameters from the end of "DRexit_line_1" to the end of "DRexit_line_2". The values of the Twiss parameters at boundaries of the doublet are given at the second and third rows of Table 4.

The matching of quadrupole doublet ("DRexit_line_2") has been initially performed using approximate analytic solutions given by Ph.J. Bryant and K. Johnsen for thin-quadrupoles [4]. Then, these solutions have been refined for thick quadrupoles using the MAD

[4] Ph.J.Bryant, K.Johnsen, "The principles of circular accelerators and storage rings", Cambr. Univ. Press, 1993.

matching commands, which utilize some numeric minimization algorithms to fit desired parameters. The analytic solutions act as design guides, because the pure numeric matching with the MAD code may require a lot of unnecessary efforts and can not guarantee an optimum and interpretable results without a guiding design. Figure 9,a shows the calculations schemes of the quadrupole doublet for the thin and thick quadrupoles at the top and the bottom, respectively.

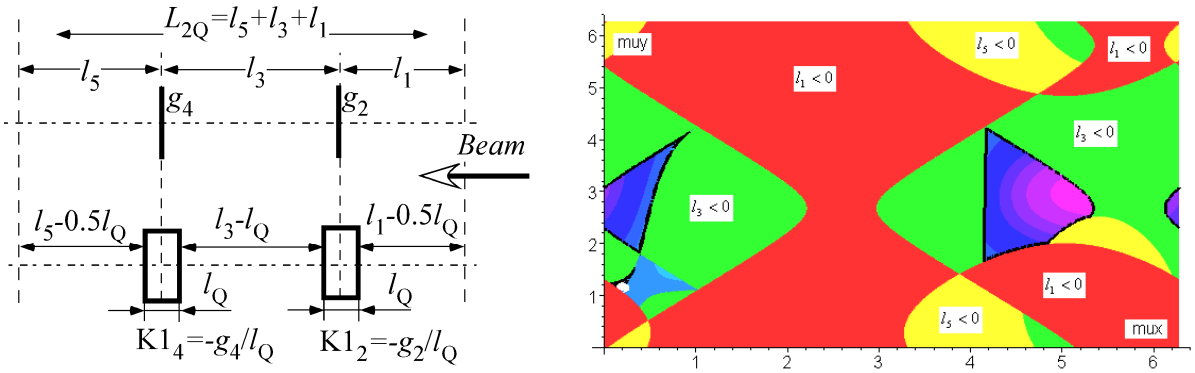

a) The schemes of the quadrupole doublets for thin and thick quadrupoles.

b) The contour plot of $F_{(4.97)}(\Delta\mu_x,\Delta\mu_y)$ for $\Delta\mu_x\in[0,2\pi]$ and $\Delta\mu_y\in[0,2\pi]$

Fig.9. Quadrupole doublet

The analytic solution for matching with the thin-quadrupole doublet is formulated using the "mismatch factor" given by the left-hand side of the Eq. 4.97 in the Ph.J. Bryant and K. Johnsen book. For a perfect solution, the "mismatch factor" denoted here as $\Phi_{(4.97)}$ must be zero. For a given values of the Twiss parameters at the doublet boundaries the function $\Phi_{(4.97)}$ depends on the phase advances $\Delta\mu_x$ and $\Delta\mu_y$ in the horizontal and vertical planes, respectively. The possible solutions are represented by the line obeying the equation $\Phi_{(4.97)}(\Delta\mu_x,\Delta\mu_y)=0$ on the $\{\Delta\mu_x,\Delta\mu_y\}$-plane. In order to exclude non-physical solutions resulting in negative lengths l_1, l_3, and l_5 and imagine gradients g_2, and g_4, the modified mismatch factor denoted as $F_{(4.97)}(\Delta\mu_x,\Delta\mu_y)$ has been introduced as the following step-wise function:

$$F_{(4.97)}(\Delta\mu_x,\Delta\mu_y)=\begin{cases}4, & \text{if } l_1<0\\ 3, & \text{if } l_5<0\\ 2, & \text{if } l_3<0\\ 1, & \text{if } \mathrm{Im}(g_{2,4})\neq 0\\ \Phi_{(4.97)}(\Delta\mu_x,\Delta\mu_y), & \text{otherwise}\end{cases}. \qquad (1)$$

Figure 9,b shows the contour plot of $F_{(4.97)}(\Delta\mu_x, \Delta\mu_y)$ over the $\{\Delta\mu_x, \Delta\mu_y\}$ area for the ranges $\Delta\mu_x \in [0,2\pi]$ and $\Delta\mu_y \in [0,2\pi]$. The areas with non-physical-physical solutions are shown by the red ($l_1 < 0$), yellow ($l_5 < 0$), and the green ($l_3 < 0$) colors, while there is no light blue areas corresponding to the imagine gradients. The areas of the physical solutions with $F_{(4.97)}(\Delta\mu_x, \Delta\mu_y) \approx 0$ occupy small blue islands.

The interior of the blue island with $\Delta\mu_x \in [0.03,1.0]$ and $\Delta\mu_y \in [0.8,1.8]$ contains the solution line $F_{(4.97)}(\Delta\mu_x, \Delta\mu_y) = 0$. Figure 10,a shows a zoomed view of this island. The black contour lines correspond to the constant values of the function $F_{(4.97)}$, which are uniformly distributed around the solution line with the step 0.01. Figure 10,b shows the solution line $F_{(4.97)}(\Delta\mu_x, \Delta\mu_y) = 0$ as the dependence $\Delta\mu_y$ vs. $\Delta\mu_x$. The solution line defines the continuous solution set. The values of the physical parameters corresponding to this solution line are shown in Fig. 11 as functions of $\Delta\mu_x$.

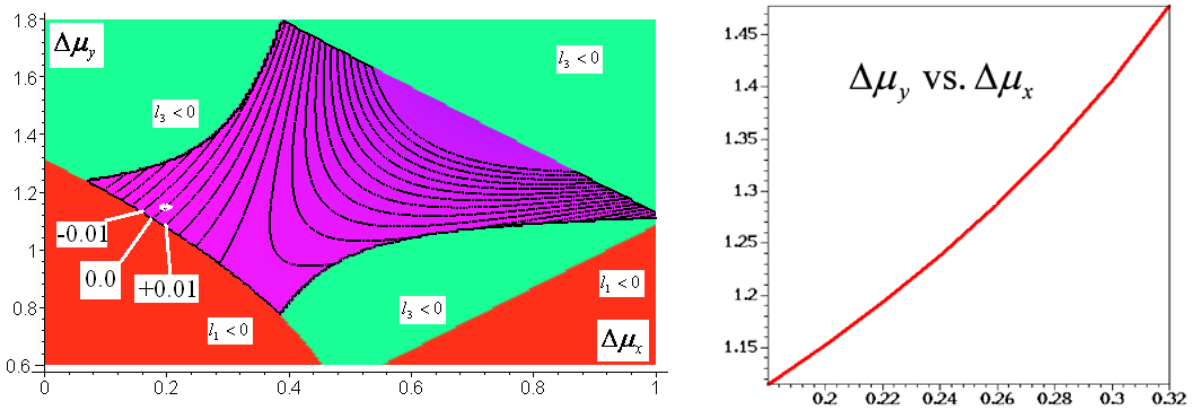

a) The contour plot of $F_{(4.97)}(\Delta\mu_x, \Delta\mu_y)$ $\Delta\mu_y$ vs. $\Delta\mu_x$ for the solution line.

Fig. 10 The function $F_{(4.97)}(\Delta\mu_x, \Delta\mu_y)$ zoomed around $\Delta\mu_x \in [0.03,1.0]$ and $\Delta\mu_y \in [0.8,1.8]$.

There is no a definite prescription for a choice of the operating point along the solution line. In a common sense, the operating point with minimal phase advances $\Delta\mu_{x,y}$ and gradients modulus $|g_{2,4}|$ and the total length l_{2Q} looks to be more preferable. The white dot in Fig. 10,a represents the example of the operating point with $\Delta\mu_x$ =0.1976 and $\Delta\mu_y$ =1.1482. This example solution provides the following physical parameters: l_1 =0.27483 m, l_3 =0.96094 m, l_5 =0.84977 m, l_{2Q} =2.0855 m, g_2 =+0.39930 m^{-1}, g_4 =-

0.61215 m^{-1}.

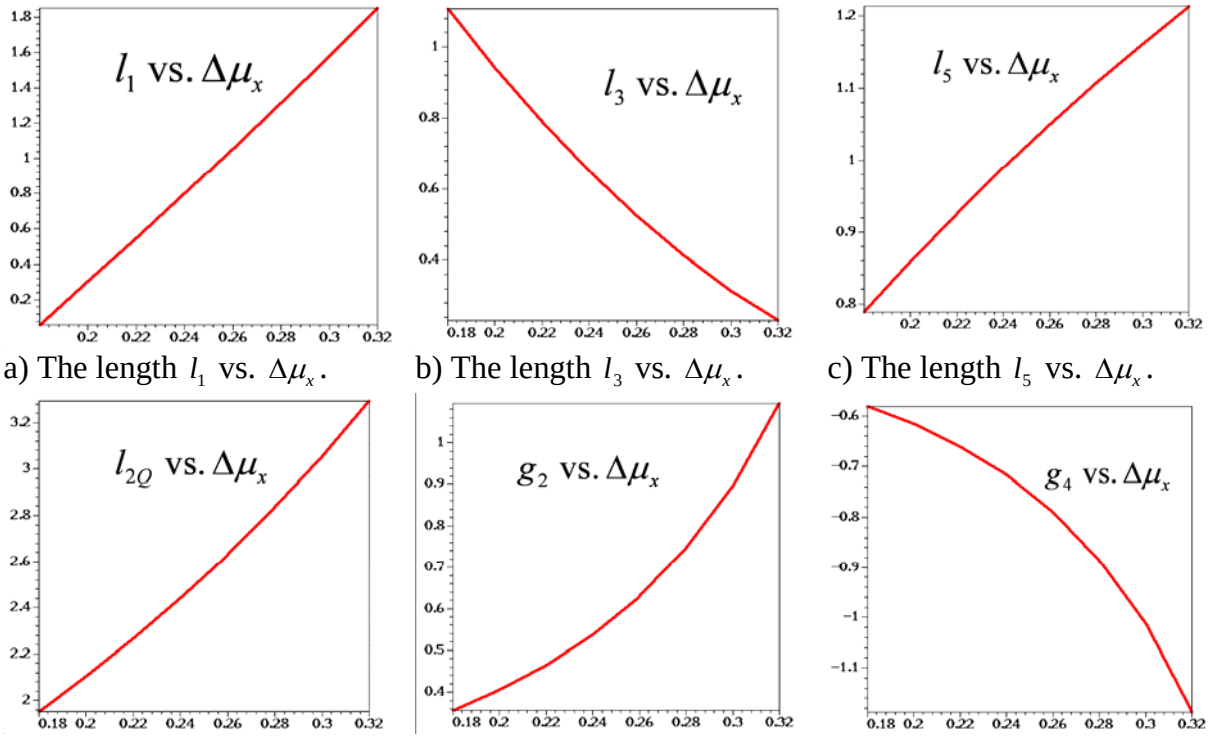

a) The length l_1 vs. $\Delta\mu_x$. b) The length l_3 vs. $\Delta\mu_x$. c) The length l_5 vs. $\Delta\mu_x$.

d) The length l_{2Q} vs. $\Delta\mu_x$. e) The gradient g_2 vs. $\Delta\mu_x$. f) The gradient g_4 vs. $\Delta\mu_x$.

Fig.11. The values of the physical parameters along the solution line as functions of $\Delta\mu_x$.

A complementary reason for the operating point choice may come from consideration of the solution sensitivity (or stability) to small deviations of initial parameters. The phase advances $\Delta\mu_{x,y}$ and the Twiss parameters $\beta_{x,y}$ and $\alpha_{x,y}$ can be assumed as such initial parameters. In terms of the phase advances, we may suggest that the low density of the contour lines in vicinity of the operating point (see Fig. 10,a) is more preferable. It looks that our operating point $\Delta\mu_x$ =0.1976 and $\Delta\mu_y$ =1.1482 obeys well to this condition.

To quantify sensitivity of the solution in terms of the Twiss parameters, let's introduce the following sensitivity matrix:

$$\delta = \begin{Vmatrix} \delta_{\beta_2}/\delta_{\beta_1} & \delta_{\beta_2}/\delta_{\alpha_1} \\ \delta_{\alpha_2}/\delta_{\beta_1} & \delta_{\alpha_2}/\delta_{\alpha_1} \end{Vmatrix}, \qquad (2)$$

where $\delta_{\beta_2}/\delta_{\beta_1}$, $\delta_{\beta_2}/\delta_{\alpha_1}$, $\delta_{\alpha_2}/\delta_{\beta_1}$, $\delta_{\alpha_2}/\delta_{\alpha_1}$ are the ratios of the relative deviations of the Twiss parameters at the doublet boundaries, while the indexes "1" and "2" denote the doublet

entrance and exit, respectively.

The elements of the sensitivity matrix has been calculated at the relative deviations of entrance Twiss parameters δ_{β_1}=1% and δ_{α_1}=1% in both x and y planes. Figure 12 shows the dependences of the matrix elements vs. the phase advance $\Delta\mu_x$.

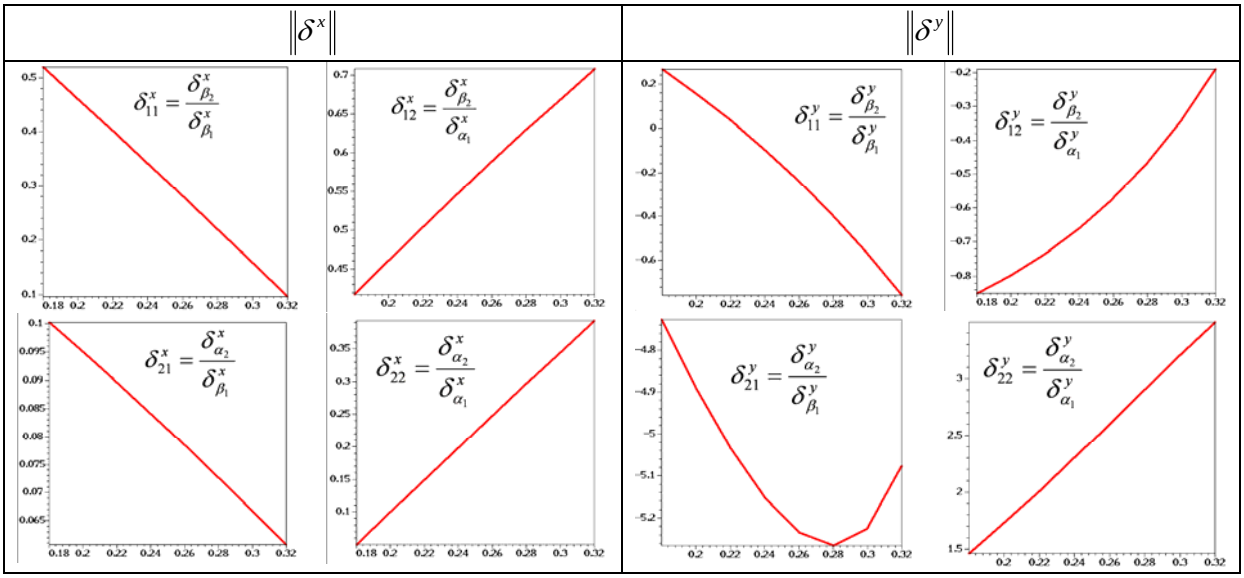

Fig.12. The sensitivity matrix elements vs. the phase advance $\Delta\mu_x$ along the solution line.

Using these curves the absolute deviations of the Twiss parameters can be derived for an operating point. Our operating point provides the following relations: $\Delta\beta_{2,x} \approx 0.8 \cdot \Delta\beta_{1,x}$, $\Delta\beta_{2,x} \approx -4.1 \cdot \Delta\alpha_{1,x}$, $\Delta\alpha_{2,x} \approx 0.05\Delta\beta_1$, $\Delta\alpha_{2,x} \approx -0.26 \cdot \Delta\alpha_{1,x}$, $\Delta\beta_{2,y} \approx 0.03 \cdot \Delta\beta_{1,y}$, $\Delta\beta_{2,y} \approx -0.8 \cdot \Delta\alpha_{1,y}$, $\Delta\alpha_{2,y} \approx 0.22 \cdot \Delta\beta_{1,y}$, $\Delta\alpha_{2,y} \approx -0.46 \cdot \Delta\alpha_{1,y}$.

The parameters of doublet derived with approximate analytical solutions for thin-quadrupoles have been refined for thick-quadrupoles of the length l_Q using the matching commands of the MAD-8 code according to the scheme shown at the bottom of Fig.9,a. The total length of quadrupole l_{2Q} was kept constant to be the same as for thin-quadrupoles, while other parameters l_1, l_3, l_5, g_2, g_4 were variable. The refining matching with MAD-8 did not meet any difficulties providing very small corrections to initial values. Similar situation took place for all other matching doublets, namely MATCH2, MATCH2a, MATCH3, MATCH4.

MATCH2 section

The MATCH2 is located between the first arc of the horizontal dogleg formed by the lines TURNMATCHR, TURNCELLR, TURNSUPPR and the EXTRACTION section. It consists of only the matching quadrupole doublet. The values of Twiss parameters at boundaries of the MATCH2 section are presented in the table below.

Table 5. Twiss parameters at boundaries of MATCH2.

position	β_x	α_x	β_y	α_y	D_x	D'_x
the entrance	10.843	-2.993	1.206	0.533	0	0
the end	47.06	-2.94	4.7	0.02	0	0

Dependence of the Twiss parameters from the beginning of “ecentral” up to the end of the EXTRACTION section is shown in Figure 13.

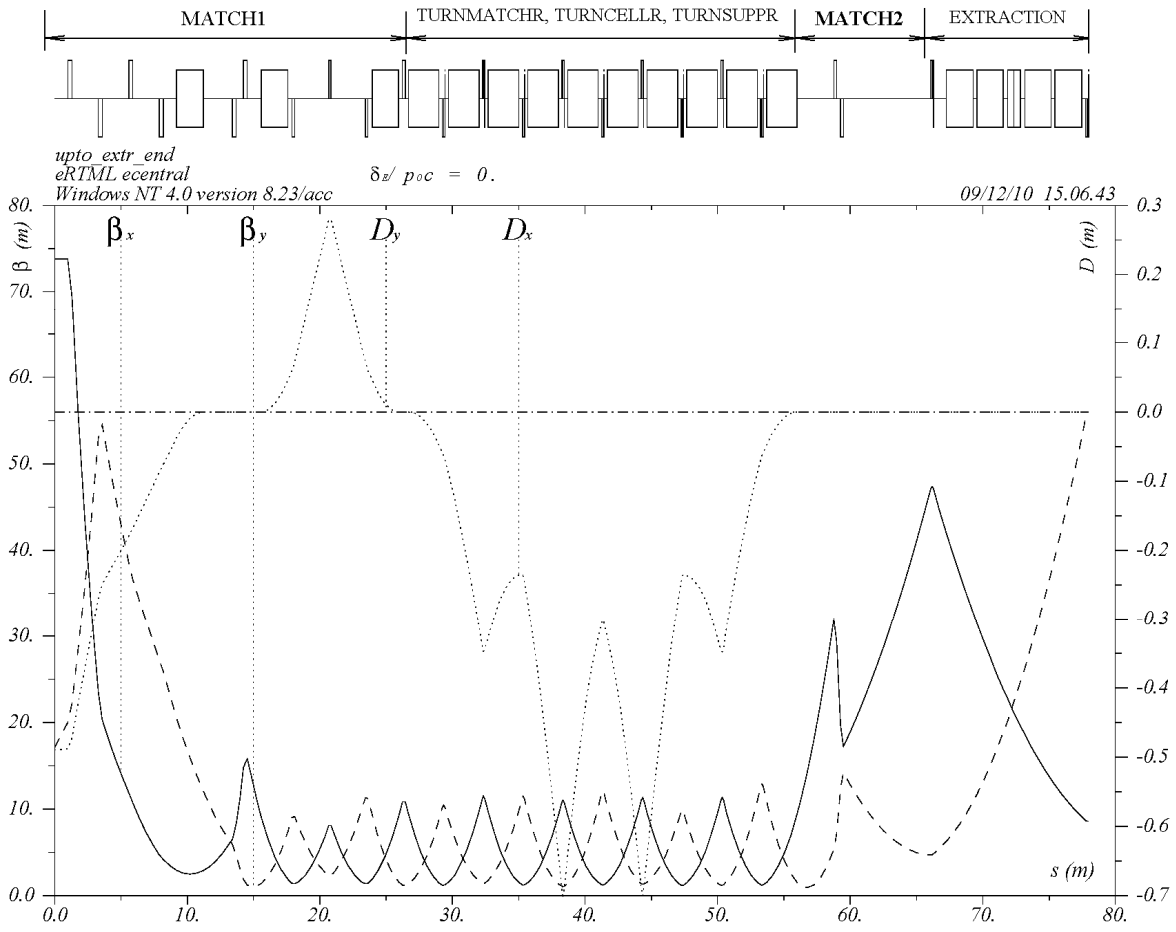

Fig. 13. The Twiss parameters $\beta_{x,y}$ and the dispersion $D_{x,y}$ shown up to the end of the EXTRACTION section.

The matching with the quadrupole doublet for the MATCH2 section has been performed similar to the quadrupole doublet of the MATCH1 section, using approximate analytic solutions and the matching commands of the MAD code.

Figure 14 shows the contour plots of $F_{(4.97)}(\Delta\mu_x, \Delta\mu_y)$ over the $\{\Delta\mu_x, \Delta\mu_y\}$ areas, while Fig.14,a shows plots over all period of the $\{\Delta\mu_x, \Delta\mu_y\}$, i.e., $\Delta\mu_x \in [0,2\pi]$ and $\Delta\mu_y \in [0,2\pi]$, and Fig.14,b shows the zoomed $\{\Delta\mu_x, \Delta\mu_y\}$ area around the blue islands with $F_{(4.97)}(\Delta\mu_x, \Delta\mu_y) \approx 0$. The black lines inside of blue areas represent zero values of $F_{(4.97)}$. Note, the bottom area does not have black lines with solutions. Two upper regions contains the black lines, and their zoomed view with contour lines is shown in Fig. 15,a.

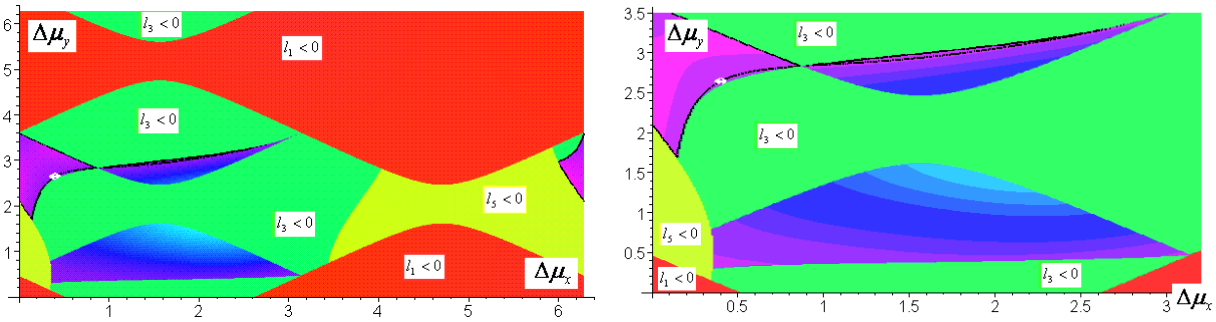

a) for $\Delta\mu_x \in [0,2\pi]$ and $\Delta\mu_y \in [0,2\pi]$ b) for $\Delta\mu_x \in [0,3.2]$ and $\Delta\mu_y \in [0,3.5]$

Fig.14. Contour plots of $F_{(4.97)}(\Delta\mu_x, \Delta\mu_y)$ for quadrupole doublet.

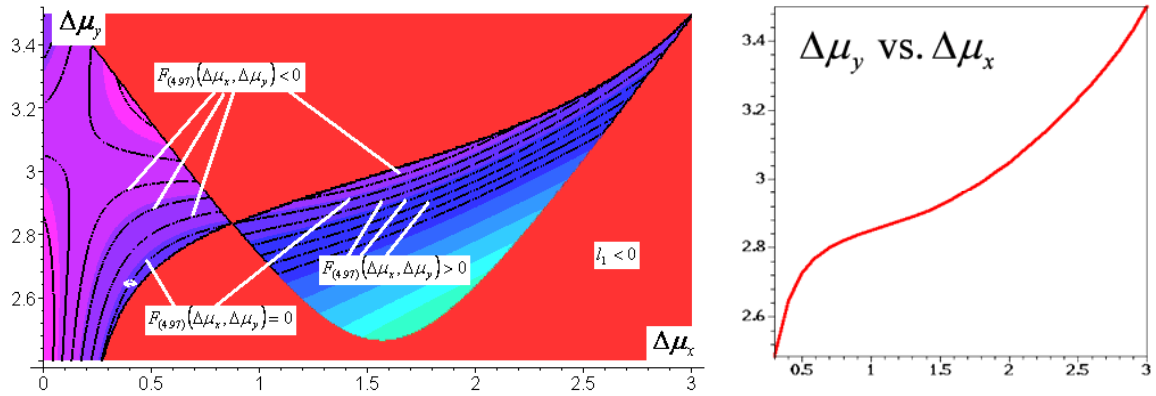

a) The contour plot of $F_{(4.97)}(\Delta\mu_x, \Delta\mu_y)$ $\Delta\mu_y$ vs. $\Delta\mu_x$ for the solution line.

Fig. 15 The function $F_{(4.97)}(\Delta\mu_x, \Delta\mu_y)$ zoomed around $\Delta\mu_x \in [0.0,3.0]$ and $\Delta\mu_y \in [2.4,3.5]$.

Figure 15,b shows the solution line $F_{(4.97)}(\Delta\mu_x, \Delta\mu_y) = 0$ as the functions of $\Delta\mu_y$ vs. $\Delta\mu_x$. The solution line defines a continuous solution set. The values of the physical parameters along this solution line are shown in Fig. 16 as functions of $\Delta\mu_x$. Figure 17

shows the dependences of the sensitivity matrix elements vs. the phase advance $\Delta\mu_x$.

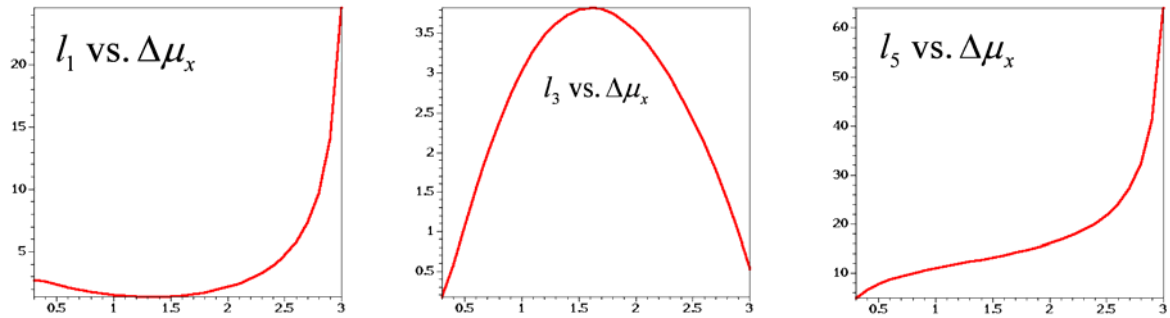

a) The length l_1 vs. $\Delta\mu_x$. b) The length l_3 vs. $\Delta\mu_x$. c) The length l_5 vs. $\Delta\mu_x$.

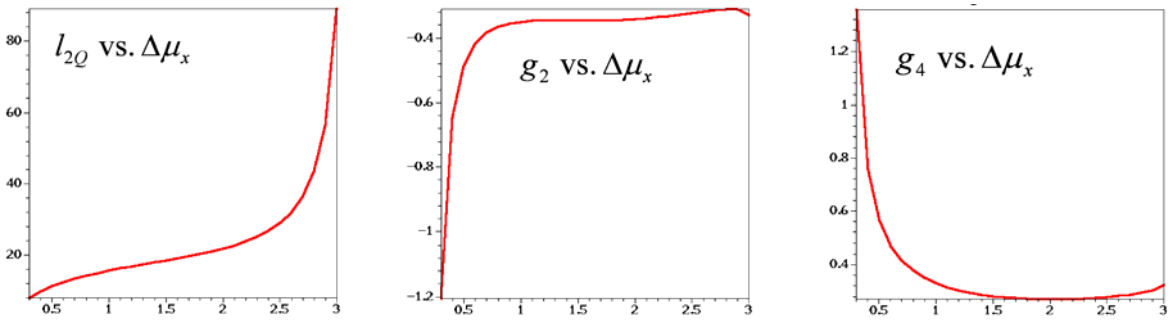

d) The length l_{2Q} vs. $\Delta\mu_x$. e) The gradient g_2 vs. $\Delta\mu_x$. f) The gradient g_4 vs. $\Delta\mu_x$.

Fig.16. The values of the physical parameters along the solution line as functions of $\Delta\mu_x$.

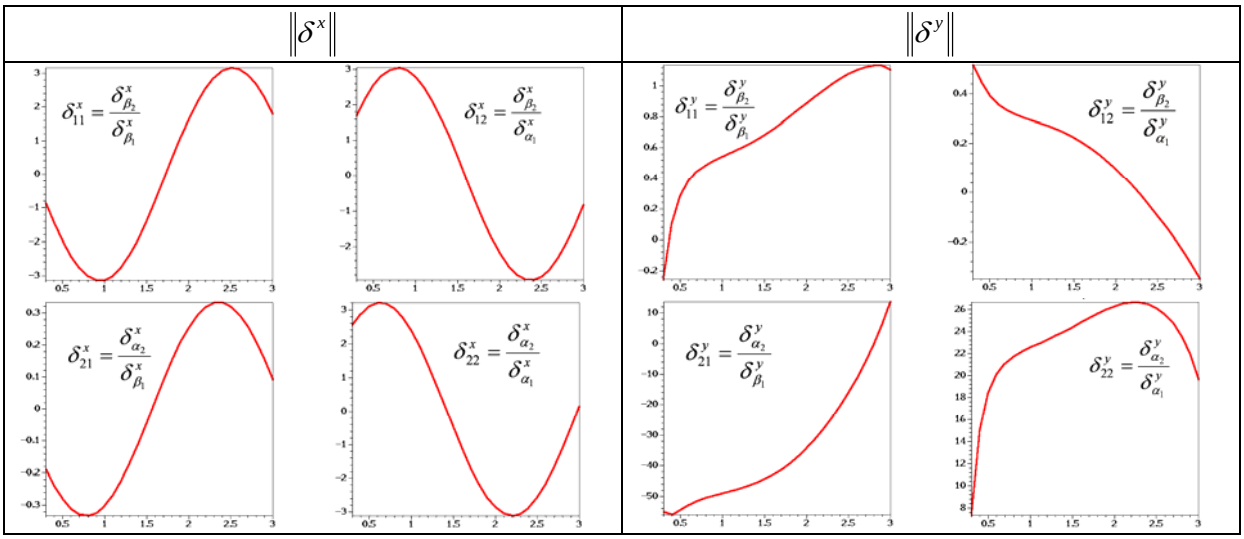

Fig.17. The sensitivity matrix elements vs. the phase advance $\Delta\mu_x$ along the solution line.

The white dots in Fig.14 and Fig. 14,a represent the example of the operating point with the phase advances $\Delta\mu_x$ =0.4 and $\Delta\mu_y$ =2.64. This example solution provides the following physical parameters: l_1 =2.591 m, l_3 =0.574 m, l_5 =6.650 m, l_{2Q} =9.815 m, g_2 =-0.647 m^{-1}, g_4 =+0.757 m^{-1}.

Using curves shown in Fig.17, the absolute deviations of the Twiss parameters can be evaluated for an operating point. Our operating point provides the following relations: $\Delta\beta_{2,x} \approx -6.3 \cdot \Delta\beta_{1,x}$, $\Delta\beta_{2,x} \approx -34.0 \cdot \Delta\alpha_{1,x}$, $\Delta\alpha_{2,x} \approx 0.07 \cdot \Delta\beta_1$, $\Delta\alpha_{2,x} \approx 2.8 \cdot \Delta\alpha_{1,x}$, $\Delta\beta_{2,y} \approx 0.39 \cdot \Delta\beta_{1,y}$, $\Delta\beta_{2,y} \approx 3.9 \cdot \Delta\alpha_{1,y}$, $\Delta\alpha_{2,y} \approx -0.93 \cdot \Delta\beta_{1,y}$, $\Delta\alpha_{2,y} \approx 0.56 \cdot \Delta\alpha_{1,y}$.

MATCH2a section

The MATCH2a is located between the EXTRACTION section and the vertical dogleg section VDOG. It consists of only the matching quadrupole doublet. The values of Twiss parameters at boundaries of the MATCH2a section are presented in the table below. Dependence of the Twiss parameters from the beginning of the EXTRACTION section up to the end of 7 cells of the VDOGFODO section is shown in Figure 18.

Table 6. Twiss parameters at boundaries of MATCH2a.

position	β_x	α_x	β_y	α_y	D_x	D'_x
the entrance	8.604	-0.294	55.627	2.384	0	0
the end	11.040	3.079	1.359	-0.340	0	0

The matching with the quadrupole doublet for the MATCH2a section has been performed similar to the quadrupole doublets of the MATCH1 and MATCH2 sections, using approximate analytic solutions and the matching commands of the MAD code.

Figure 19 shows the contour plots of $F_{(4.97)}(\Delta\mu_x, \Delta\mu_y)$ over the $\{\Delta\mu_x, \Delta\mu_y\}$ areas, while Fig.19,a shows plots over all period of the $\{\Delta\mu_x, \Delta\mu_y\}$ for the ranges $\Delta\mu_x \in [0,2\pi]$ and $\Delta\mu_y \in [0,2\pi]$. The black lines represent zero values of the function $F_{(4.97)}(\Delta\mu_x, \Delta\mu_y)$. There are three blue islands with $F_{(4.97)}(\Delta\mu_x, \Delta\mu_y) \approx 0$, and only left-bottom blue island has black line inside it. Fig.19,b shows the $\{\Delta\mu_x, \Delta\mu_y\}$ area zoomed around two left blue islands with $F_{(4.97)}(\Delta\mu_x, \Delta\mu_y) \approx 0$. Note, the upper-left area does not have internal black lines with zeroes of the function $F_{(4.97)}(\Delta\mu_x, \Delta\mu_y)$, i.e., this area does not contain solutions. The left-bottom area containing internal the black lines, and their zoomed view with contour lines are shown in Fig. 20,a.

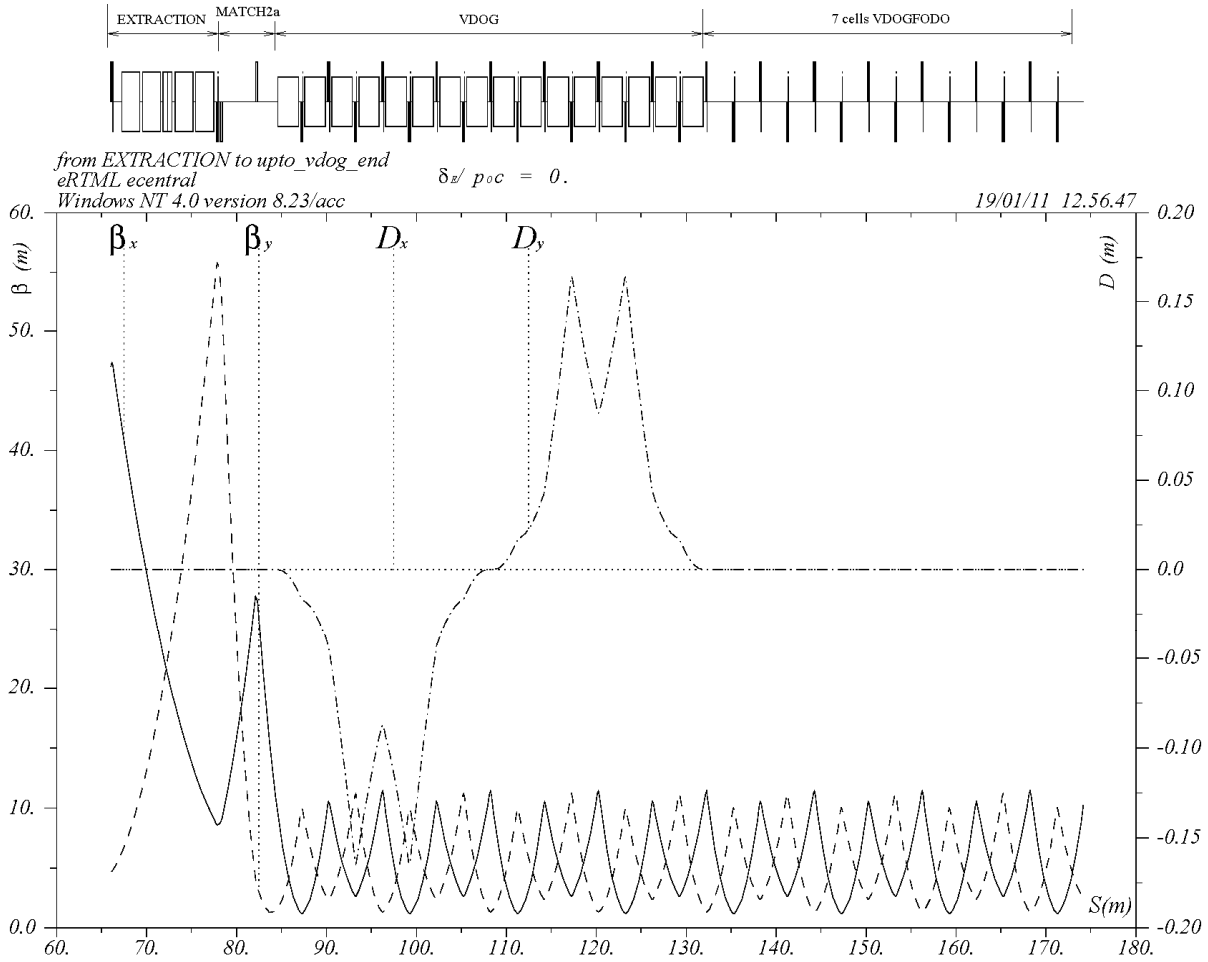

Fig. 18. The Twiss parameters $\beta_{x,y}$ and the dispersion $D_{x,y}$ shown from the EXTRACTION section to the end of 7 cells of the VDOGFODO section.

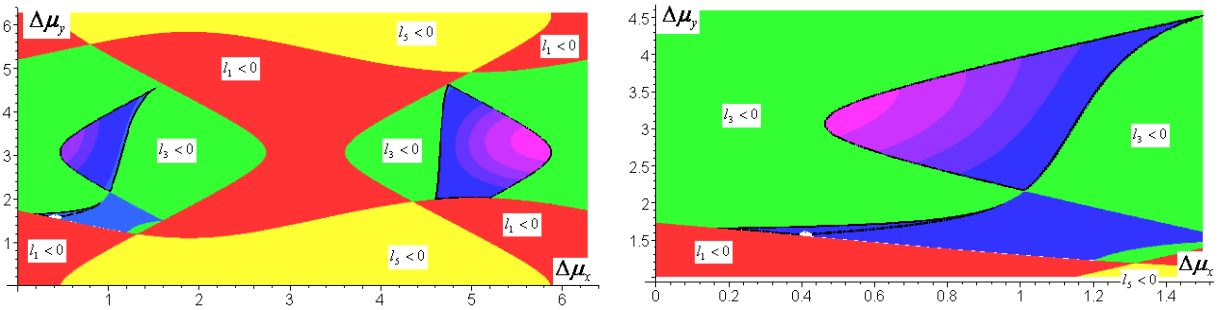

a) for $\Delta\mu_x \in [0,2\pi]$ and $\Delta\mu_y \in [0,2\pi]$ b) for $\Delta\mu_x \in [0,1.5]$ and $\Delta\mu_y \in [1.0,4.7]$

Fig.19. Contour plots of $F_{(4.97)}(\Delta\mu_x, \Delta\mu_y)$ for quadrupole doublet.

Figure 20,b shows the solution line $F_{(4.97)}(\Delta\mu_x, \Delta\mu_y) = 0$ as the dependence $\Delta\mu_y$ vs. $\Delta\mu_x$. The solution line defines the continuous solution set. The values of the physical parameters corresponding to this solution line are shown in Fig. 21 as functions of the phase

advance $\Delta\mu_x$. Figure 22 shows the dependences for the sensitivity matrix elements vs. the phase advance $\Delta\mu_x$.

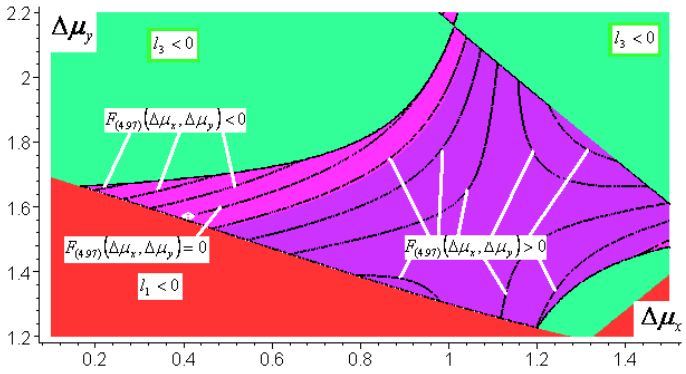

a) The contour plot of $F_{(4.97)}(\Delta\mu_x, \Delta\mu_y)$

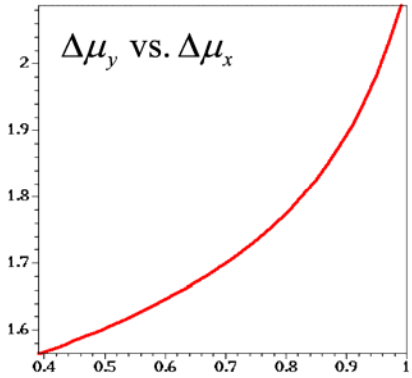

$\Delta\mu_y$ vs. $\Delta\mu_x$ for the solution line.

Fig. 20. The function $F_{(4.97)}(\Delta\mu_x, \Delta\mu_y)$ zoomed around $\Delta\mu_x \in [0.1,1.5]$ and $\Delta\mu_y \in [1.2,2.2]$.

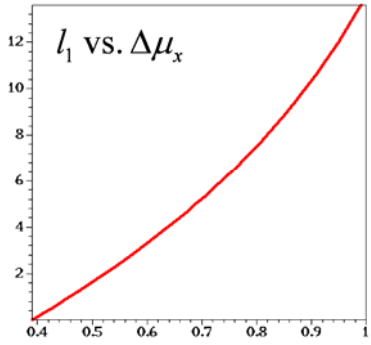

a) The length l_1 vs. $\Delta\mu_x$.

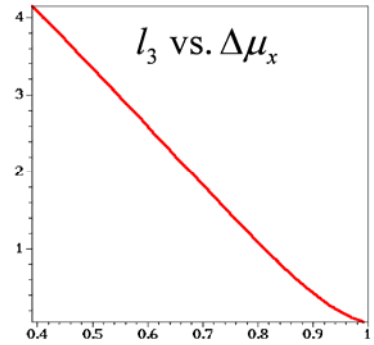

b) The length l_3 vs. $\Delta\mu_x$.

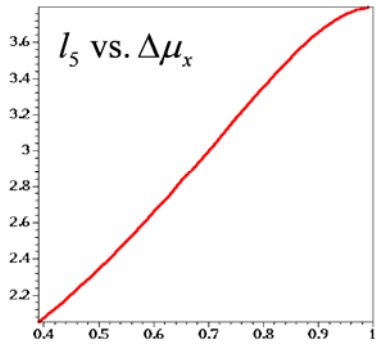

c) The length l_5 vs. $\Delta\mu_x$.

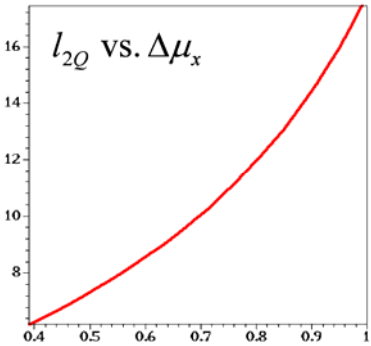

d) The length l_{2Q} vs. $\Delta\mu_x$.

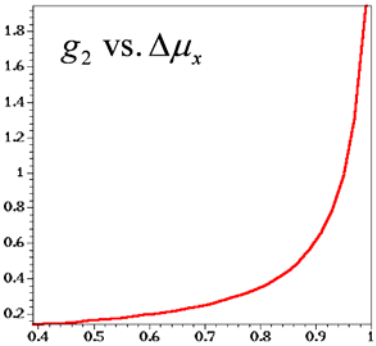

e) The gradient g_2 vs. $\Delta\mu_x$.

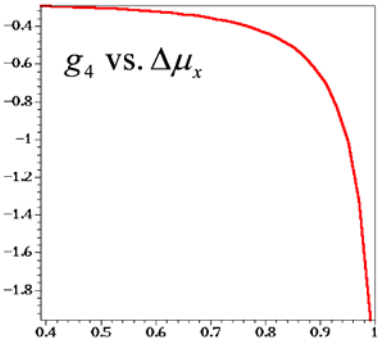

f) The gradient g_4 vs. $\Delta\mu_x$.

Fig.21. The values of the physical parameters along the solution line as functions of $\Delta\mu_x$.

The white dots in Fig.19 and Fig. 20,a represent the example of the operating point with the phase advances $\Delta\mu_x$ =0.41 and $\Delta\mu_y$ =1.57. This example solution provides the following physical parameters: l_1 =0.290 m, l_3 =4.001 m, l_5 =2.102 m, l_{2Q} =6.394 m,

g_2 =0.145 m^{-1}, g_4 =-0.295 m^{-1}.

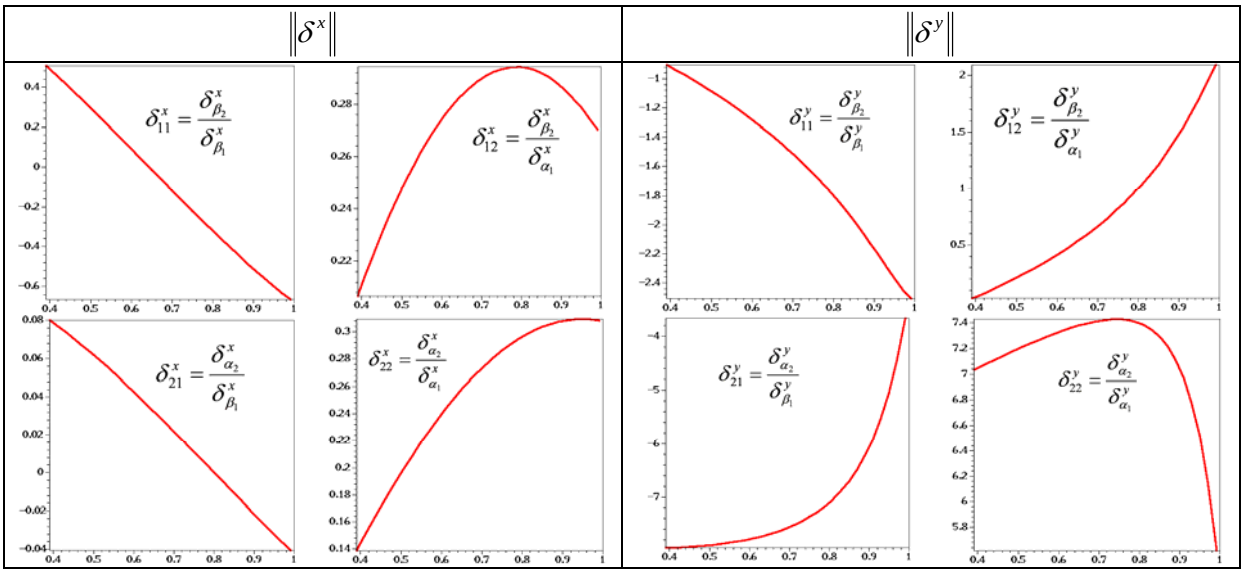

Fig.22. The sensitivity matrix elements vs. the phase advance $\Delta\mu_x$ along the solution line.

Using curves shown in Fig.22, the absolute deviations of the Twiss parameters can be derived for an operating point. Our operating point provides the following relations: $\Delta\beta_{2,x} \approx 0.47 \cdot \Delta\beta_{1,x}$, $\Delta\beta_{2,x} \approx -8.1 \cdot \Delta\alpha_{1,x}$, $\Delta\alpha_{2,x} \approx 0.028 \cdot \Delta\beta_1$, $\Delta\alpha_{2,x} \approx -1.6 \cdot \Delta\alpha_{1,x}$, $\Delta\beta_{2,y} \approx -0.023 \cdot \Delta\beta_{1,y}$, $\Delta\beta_{2,y} \approx 0.034 \cdot \Delta\alpha_{1,y}$, $\Delta\alpha_{2,y} \approx 0.049 \cdot \Delta\beta_{1,y}$, $\Delta\alpha_{2,y} \approx 1.0 \cdot \Delta\alpha_{1,y}$.

MATCH3 section

The MATCH3 section is located between the VDOGFODO section and the second arc of the horizontal dogleg section formed by the lines TURNMATCH, TURNCELL, TURNSUPP. The MATCH3 section consists of three quadrupoles. The first quadrupole is added at the entrance of the MATCH3 as a continuation of the VDOGFODO section in order preserve the beam size at the entrance of the following quadrupole doublet formed by the second and third quadrupoles of the MATCH3 section. The values of Twiss parameters at boundaries of the MATCH3 section are presented in the table below. Dependence of the Twiss parameters in the MATCH3 section and its adjacent sections is shown in Figure 23.

The matching with the quadrupole doublet of the MATCH3 section has been performed similar to the quadrupole doublets of the MATCH1, MATCH2, MATCH2a sections, using approximate analytic solutions and the MAD code matching commands.

Table 7. Twiss parameters at boundaries of the MATCH3 section.

position	β_x	α_x	β_y	α_y	D_x	D'_x
the entrance	10.368	2.104	2.440	-0.685	0	0
the end	11.040	3.079	1.359	-0.340	0	0

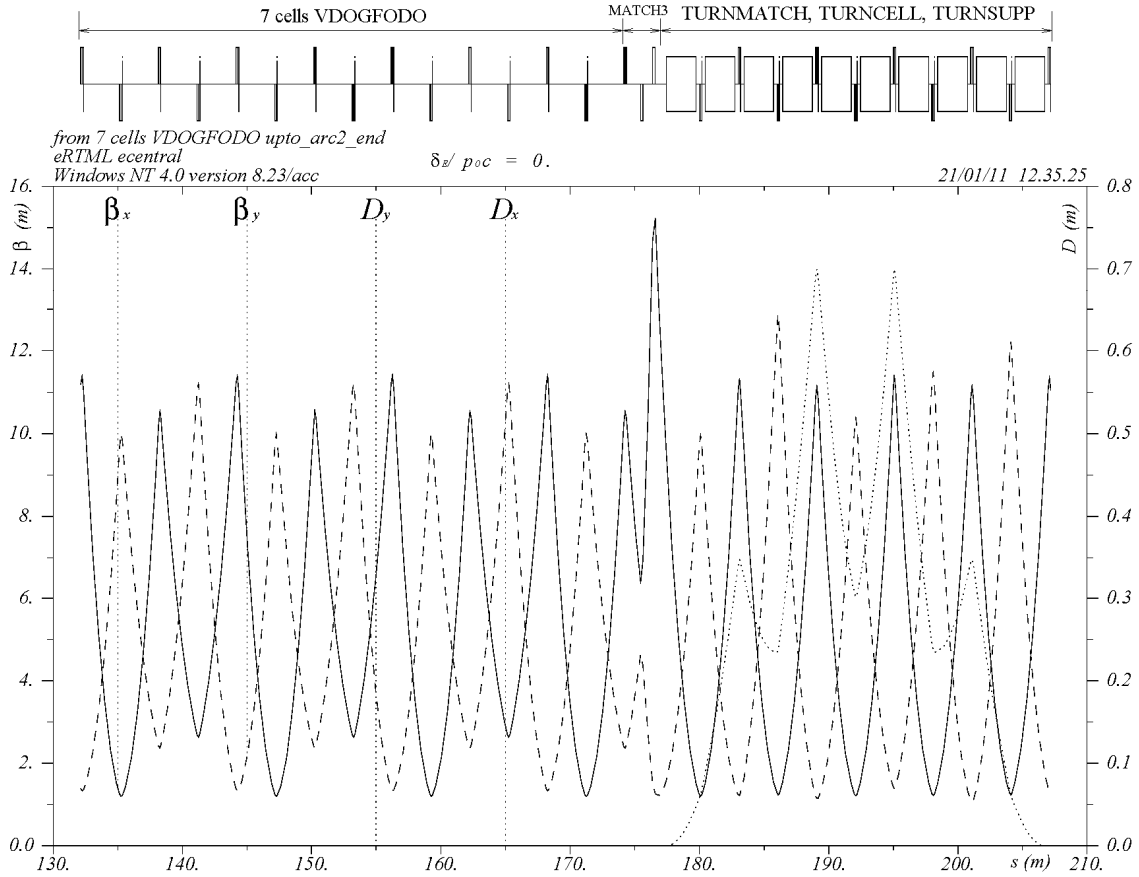

Fig. 23. The Twiss parameters $\beta_{x,y}$ and the dispersion $D_{x,y}$ shown from the VDOGFODO section to the end of the second arc of the horizontal dogleg.

Figure 24 shows the contour plots of $F_{(4.97)}(\Delta\mu_x, \Delta\mu_y)$ over the $\{\Delta\mu_x, \Delta\mu_y\}$ areas, while Fig.24,a shows plots over all period of the $\{\Delta\mu_x, \Delta\mu_y\}$ for the ranges $\Delta\mu_x \in [0,2\pi]$ and $\Delta\mu_y \in [0,2\pi]$. The black lines represent zero values of the function $F_{(4.97)}(\Delta\mu_x, \Delta\mu_y)$. There are three blue islands with $F_{(4.97)}(\Delta\mu_x, \Delta\mu_y) \approx 0$, while two of them contain the internal black solution line which is actually common for both islands. Fig.24,b shows the $\{\Delta\mu_x, \Delta\mu_y\}$ area zoomed around two blue islands with the common solution line. The detailed zoomed view of these islands with contour lines is shown in Fig. 25,a.

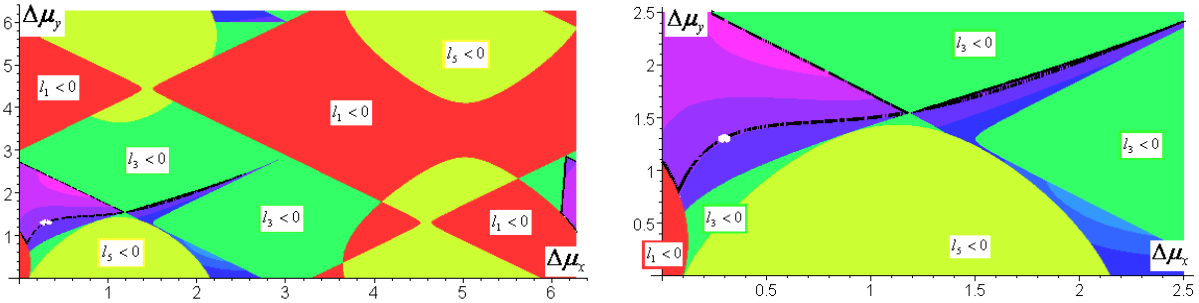

a) for $\Delta\mu_x \in [0,2\pi]$ and $\Delta\mu_y \in [0,2\pi]$ b) for $\Delta\mu_x \in [0,2.5]$ and $\Delta\mu_y \in [0.0,2.5]$

Fig.24. Contour plots of $F_{(4.97)}(\Delta\mu_x, \Delta\mu_y)$ for quadrupole doublet.

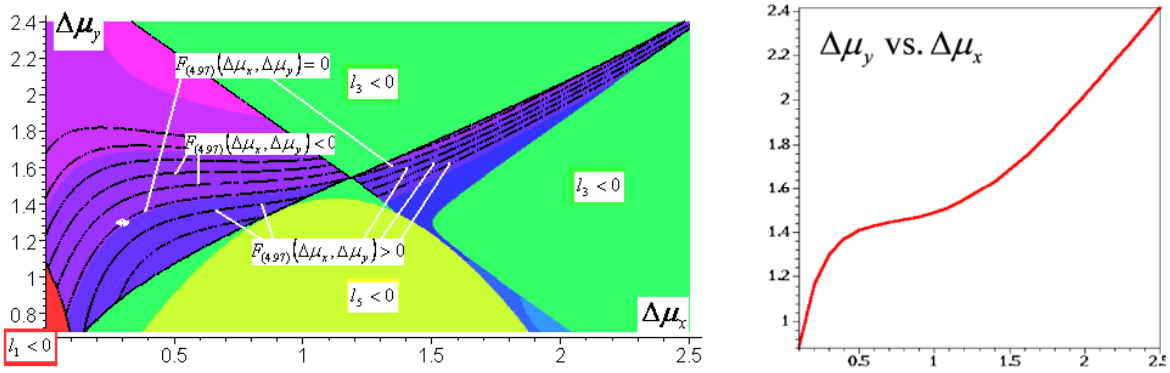

a) The contour plot of $F_{(4.97)}(\Delta\mu_x, \Delta\mu_y)$ $\Delta\mu_y$ vs. $\Delta\mu_x$ for the solution line.

Fig. 25. The function $F_{(4.97)}(\Delta\mu_x, \Delta\mu_y)$ zoomed around $\Delta\mu_x \in [0.0,2.5]$ and $\Delta\mu_y \in [0.7,2.4]$.

Figure 25,b shows the solution line $F_{(4.97)}(\Delta\mu_x, \Delta\mu_y) = 0$ as the dependence $\Delta\mu_y$ vs. $\Delta\mu_x$. The solution line defines the continuous solution set. The values of the physical parameters corresponding to this solution line are shown in Fig. 26 as functions of the phase advance $\Delta\mu_x$. Figure 27 shows the dependences for the sensitivity matrix elements vs. the phase advance $\Delta\mu_x$.

The white dots in Fig.24 and Fig. 25,a represent the example of the operating point with the phase advances $\Delta\mu_x$ =0.300 and $\Delta\mu_y$ =1.299. This example solution provides the following physical parameters: l_1 =1.160 m, l_3 =1.014 m, l_5 =0.667 m, l_{2Q} =2.842 m, g_2 =0.810 m^{-1}, g_4 =-0.606 m^{-1}.

Using curves shown in Fig.27, the absolute deviations of the Twiss parameters can be evaluated for an operating point. Our operating point provides the following relations: $\Delta\beta_{2,x} \approx 1.9 \cdot \Delta\beta_{1,x}$, $\Delta\beta_{2,x} \approx -10.6 \cdot \Delta\alpha_{1,x}$, $\Delta\alpha_{2,x} \approx 0.07 \cdot \Delta\beta_1$, $\Delta\alpha_{2,x} \approx -3.2 \cdot \Delta\alpha_{1,x}$, $\Delta\beta_{2,y} \approx -0.61 \cdot \Delta\beta_{1,y}$, $\Delta\beta_{2,y} \approx -0.27 \cdot \Delta\alpha_{1,y}$, $\Delta\alpha_{2,y} \approx -0.04 \cdot \Delta\beta_{1,y}$, $\Delta\alpha_{2,y} \approx -0.91 \cdot \Delta\alpha_{1,y}$.

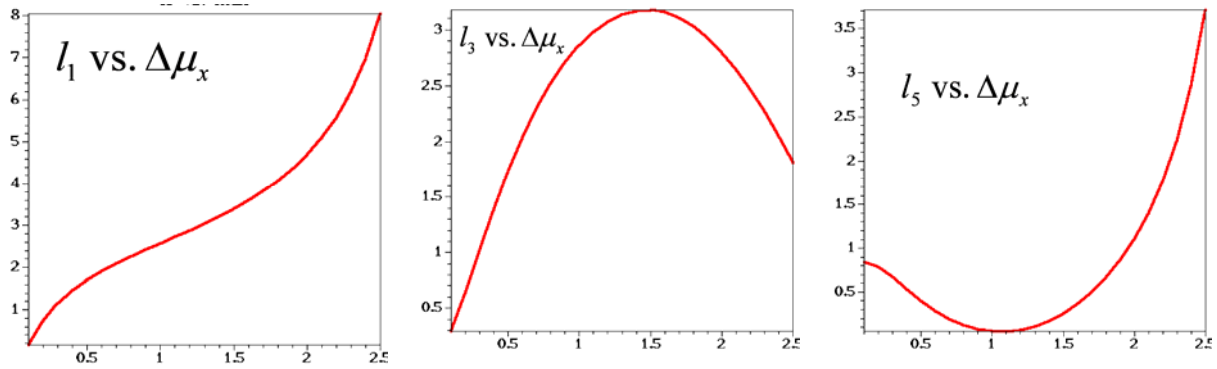

a) The length l_1 vs. $\Delta\mu_x$. b) The length l_3 vs. $\Delta\mu_x$. c) The length l_5 vs. $\Delta\mu_x$.

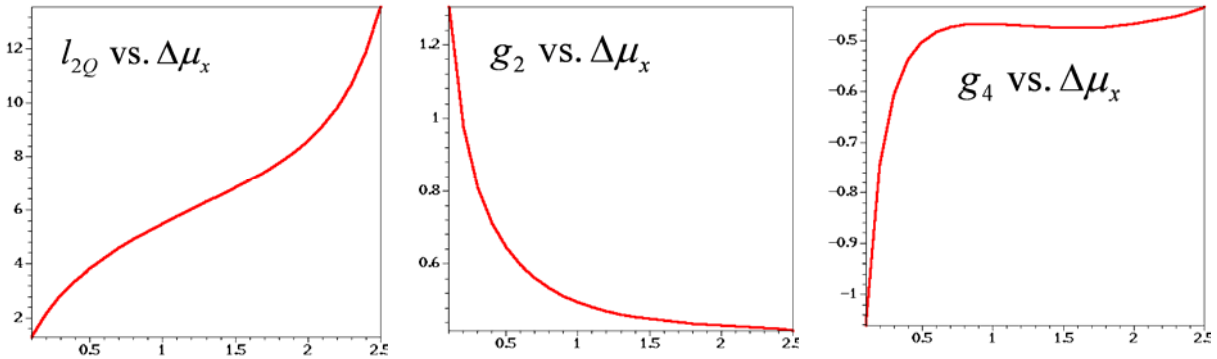

d) The length l_{2Q} vs. $\Delta\mu_x$. e) The gradient g_2 vs. $\Delta\mu_x$. f) The gradient g_4 vs. $\Delta\mu_x$.

Fig.26. The values of the physical parameters along the solution line as functions of $\Delta\mu_x$.

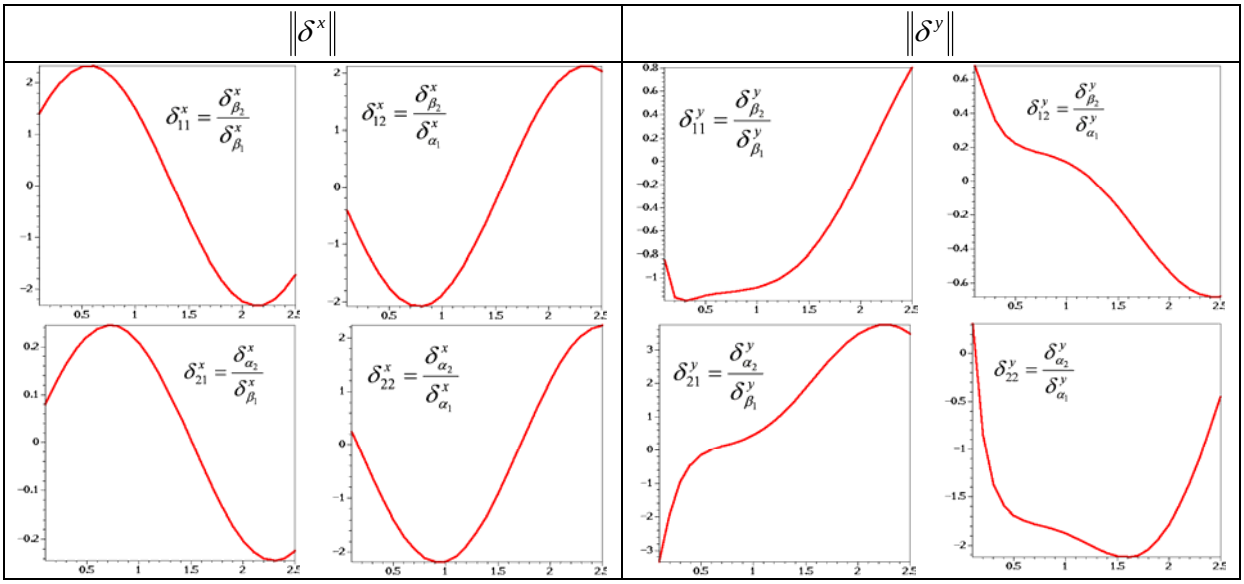

Fig.27. The sensitivity matrix elements vs. the phase advance $\Delta\mu_x$ along the solution line.

MATCH4 section

The MATCH4 section is located between the second arc of the horizontal dogleg section and the match to the skew section. The MATCH4 section consists of only the matching quadrupole doublet. The values of Twiss parameters at boundaries of the MATCH4 section are presented in the table below. Dependence of the Twiss parameters in the MATCH4 section and its adjacent sections is shown in Figure 28.

Table 8. Twiss parameters at boundaries of the MATCH4 section.

position	β_x	α_x	β_y	α_y	D_x	D'_x
the entrance	11.040	3.078	1.360	-0.342	0	0
the end	1.630	0.481	9.341	-2.626	0	0

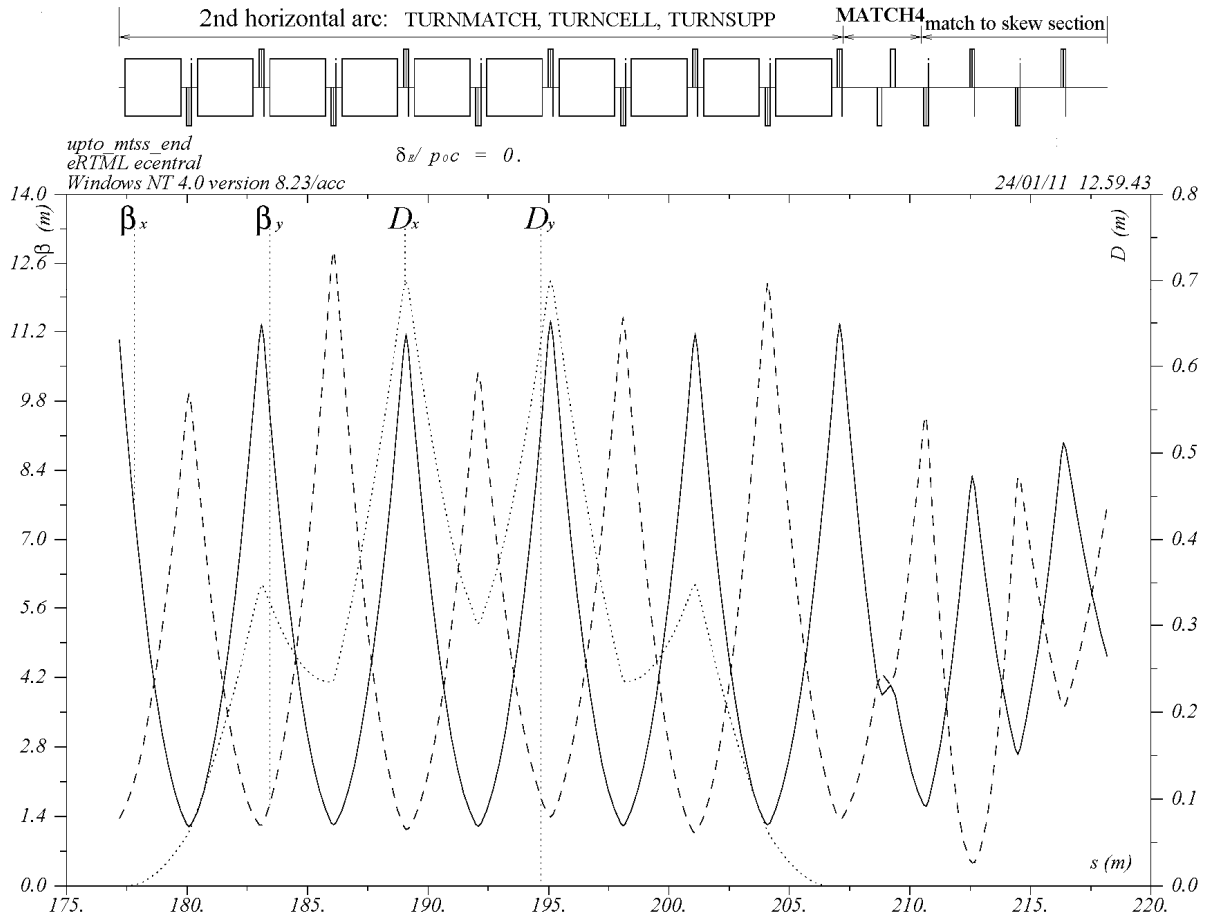

Fig. 28. The Twiss parameters $\beta_{x,y}$ and the dispersion $D_{x,y}$ shown from the second arc of the horizontal dogleg section to the match to the skew section.

The matching with the quadrupole doublet of the MATCH4 section has been

performed similar to the quadrupole doublets of the MATCH1, MATCH2, MATCH2a, MATCH4 sections, using approximate analytic solutions and the MAD code matching commands.

Figure 29 shows the contour plots of $F_{(4.97)}(\Delta\mu_x, \Delta\mu_y)$ over the $\{\Delta\mu_x, \Delta\mu_y\}$ areas, while Fig.29,a shows plots over all period of the $\{\Delta\mu_x, \Delta\mu_y\}$ for the ranges $\Delta\mu_x \in [0,2\pi]$ and $\Delta\mu_y \in [0,2\pi]$. The black lines represent zero values of the function $F_{(4.97)}(\Delta\mu_x, \Delta\mu_y)$. There are two blue islands with $F_{(4.97)}(\Delta\mu_x, \Delta\mu_y) \approx 0$ .Fig.29,b shows the $\{\Delta\mu_x, \Delta\mu_y\}$ area zoomed around two blue islands with several contour lines.

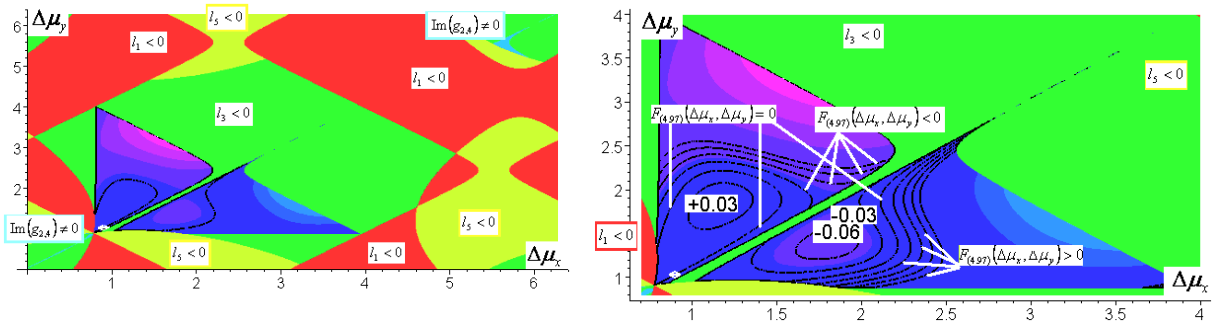

a) for $\Delta\mu_x \in [0,2\pi]$ and $\Delta\mu_y \in [0,2\pi]$ b) for $\Delta\mu_x \in [0.7,4.0]$ and $\Delta\mu_y \in [0.8,4.0]$

Fig.29. Contour plots of $F_{(4.97)}(\Delta\mu_x, \Delta\mu_y)$ for quadrupole doublet.

The solution lines of two islands are two bent curves, providing two double-valued dependences for the solution function $\Delta\mu_y = f(\Delta\mu_x)$. Let's present these dependences as four one-valued functions, corresponding to four separated branches of the function. Figure 30 shows the four dependences $\Delta\mu_y = f(\Delta\mu_x)$ for four branches of the function. Fig.30,a and Fig.30,b show lower and upper branches of the solution line belonging to the left blue island, respectively. Fig.30,c and Fig.30,d show the function $\Delta\mu_y = f(\Delta\mu_x)$ for the solution line located on the right blue island. The function has a negative derivative in the segment with $\Delta\mu_x \in [2.1,2.2]$, resulting in a double-valued dependence there. Therefore, Fig.30,c shows two segments of the function $\Delta\mu_y = f(\Delta\mu_x)$ with a positive derivative, and Fig.30,d show segment of the function $\Delta\mu_y = f(\Delta\mu_x)$ with a negative derivative.

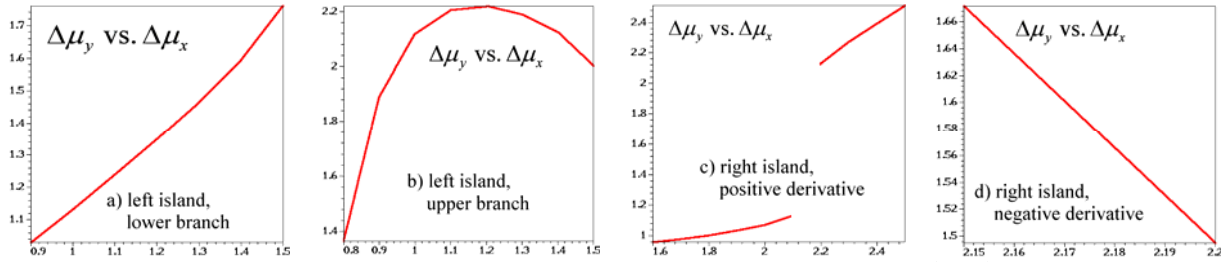

Fig.30. Four branches of the solution function $\Delta\mu_y = f(\Delta\mu_x)$.

The dependences of the physical parameters corresponding to four branches of the solution function $\Delta\mu_y = f(\Delta\mu_x)$ are shown in Fig.31-36 as functions of the phase advance $\Delta\mu_x$. The dependences for the sensitivity matrix elements on the phase advances are shown in Fig.37-40 for every of four branches of the solution lines.

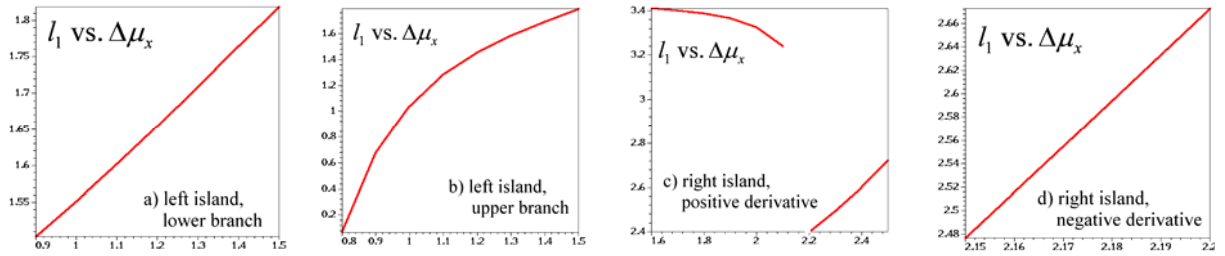

Fig.31. Four branches of the function $l_1 = f(\Delta\mu_x)$.

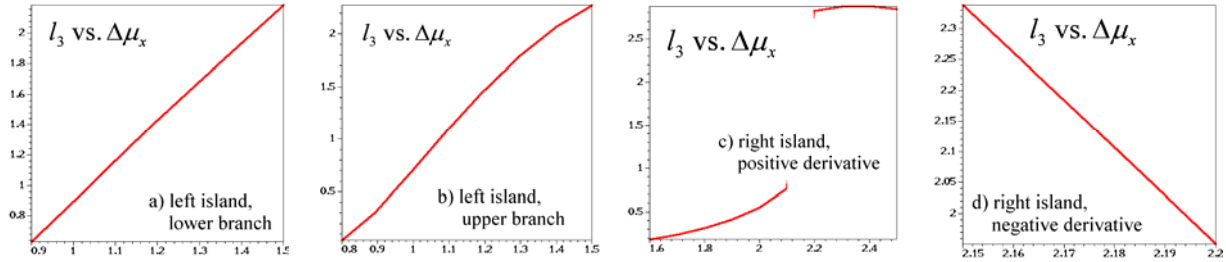

Fig.32. Four branches of the function $l_3 = f(\Delta\mu_x)$.

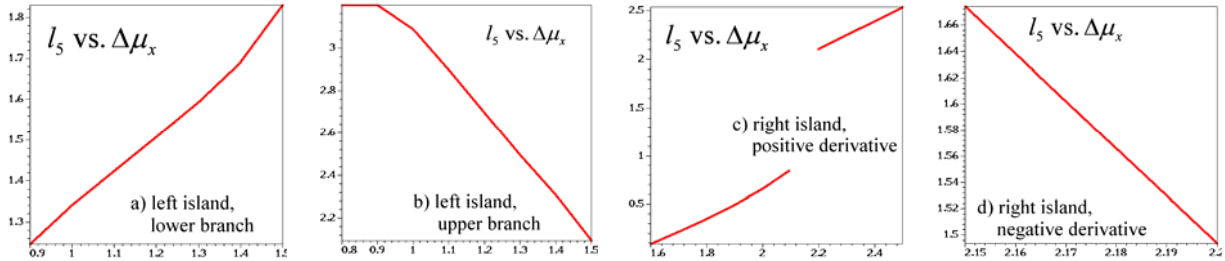

Fig.33. Four branches of the function $l_5 = f(\Delta\mu_x)$.

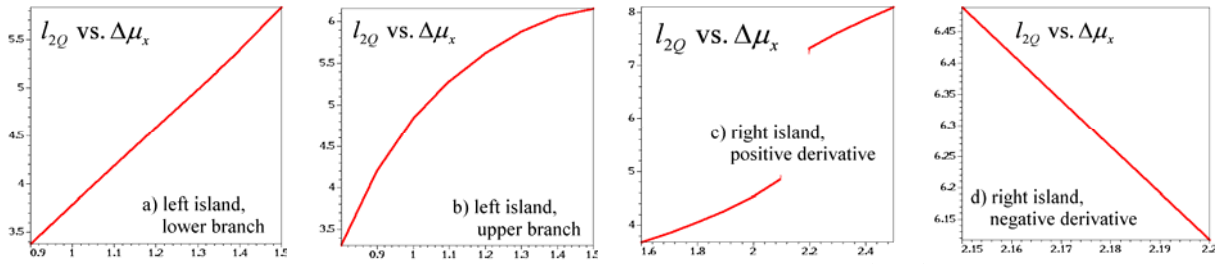

Fig.34. Four branches of the function $l_{2Q} = f(\Delta\mu_x)$.

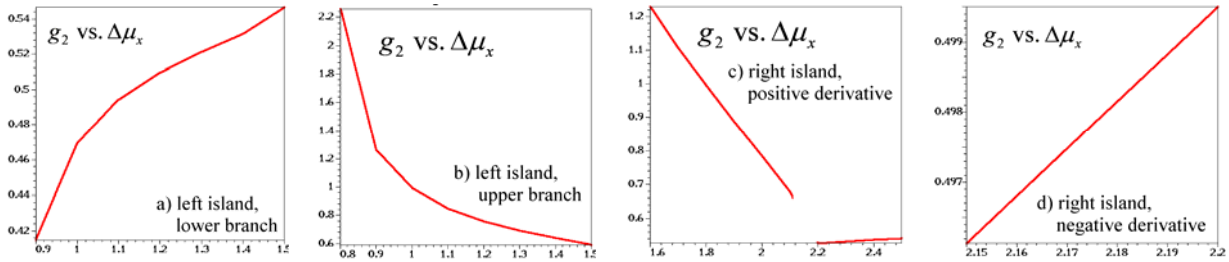

Fig.35. Four branches of the function $g_2 = f(\Delta\mu_x)$.

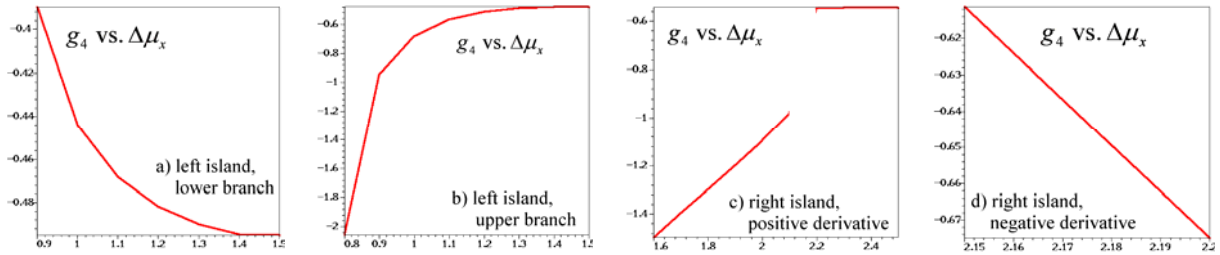

Fig.36. Four branches of the function $g_4 = f(\Delta\mu_x)$.

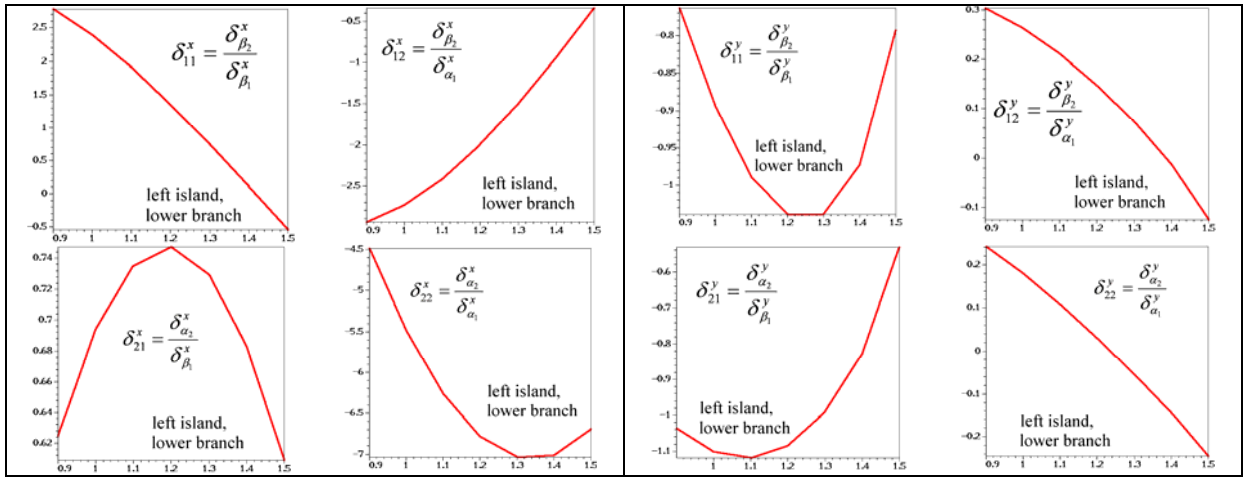

Fig.37. The elements of $\|\delta^x\|$ and $\|\delta^y\|$ vs. $\Delta\mu_x$ line for the 1st branch of the solution line.

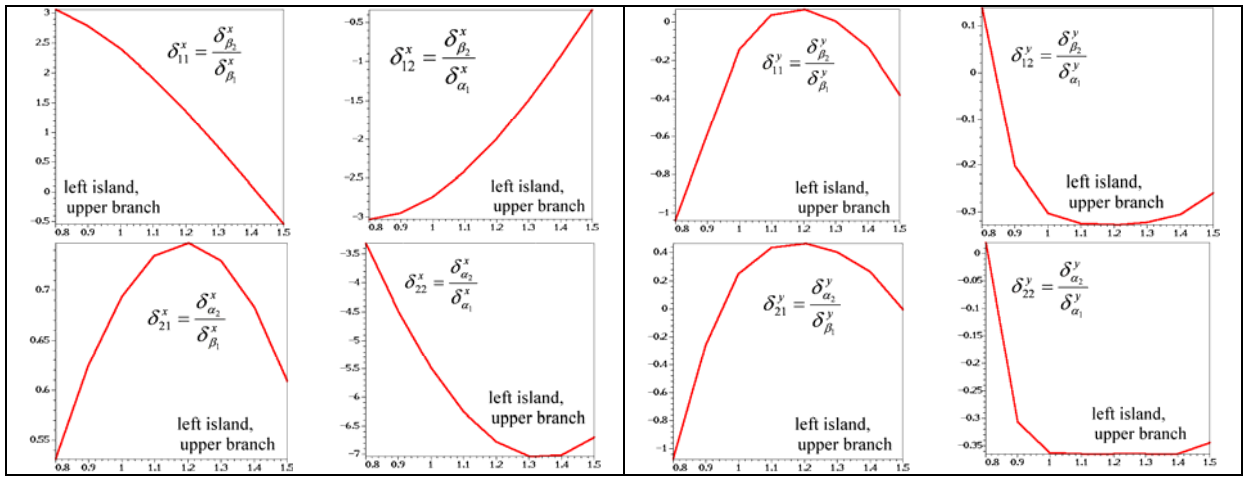

Fig.38. The elements of $\|\delta^x\|$ and $\|\delta^y\|$ vs. $\Delta\mu_x$ line for the 2nd branch of the solution line.

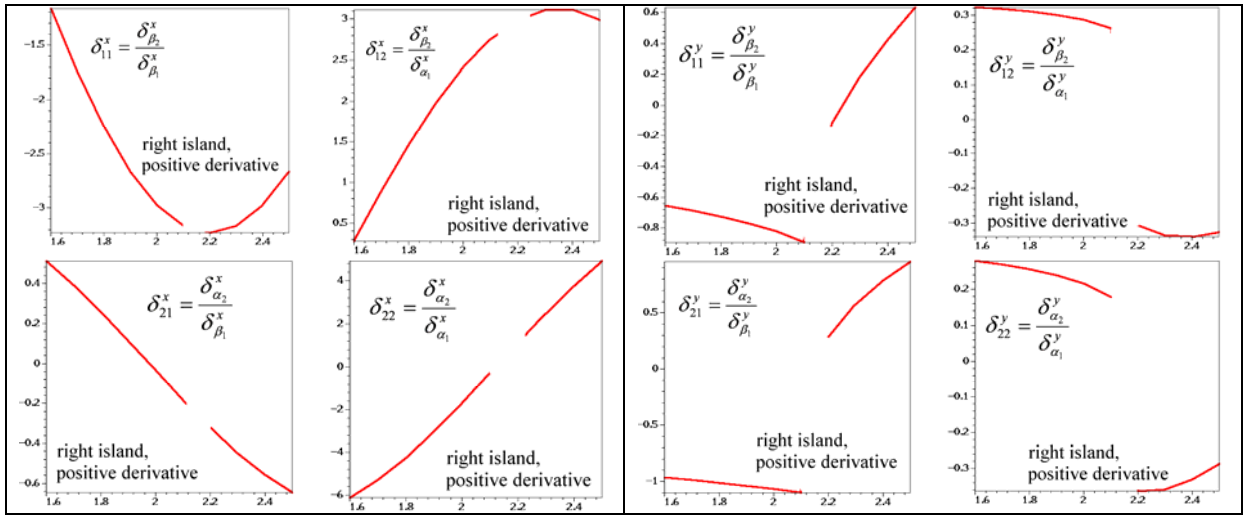

Fig.39. The elements of $\|\delta^x\|$ and $\|\delta^y\|$ vs. $\Delta\mu_x$ line for the 3rd branch of the solution line.

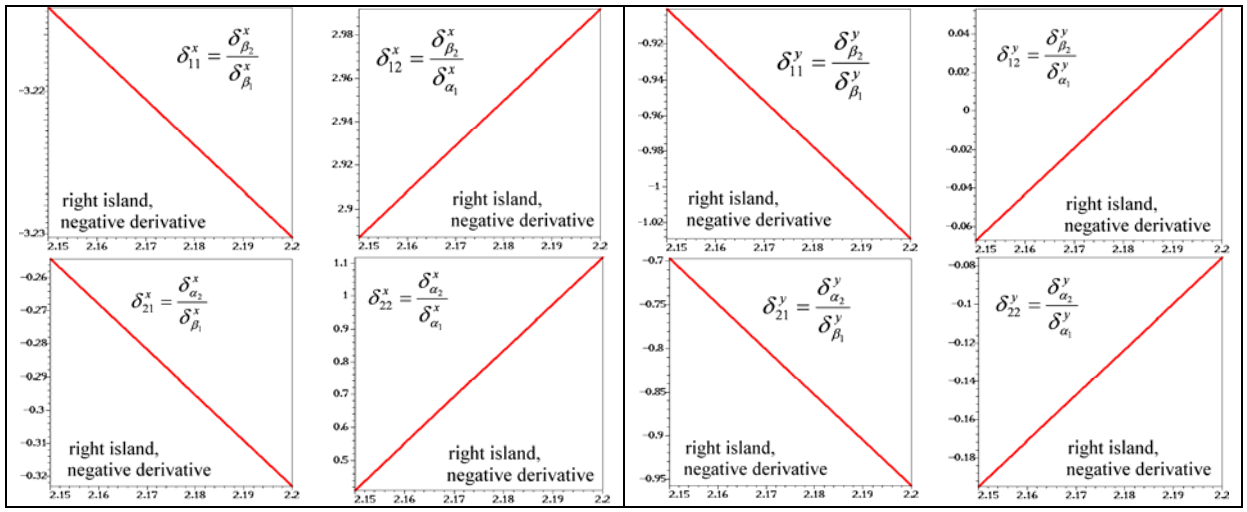

Fig.40. The elements of $\|\delta^x\|$ and $\|\delta^y\|$ vs. $\Delta\mu_x$ line for the 4th branch of the solution line.

The white dots in Fig.29 represent the example of the operating point with the phase advances $\Delta\mu_x$ =0.90 and $\Delta\mu_y$ =1.03. This example solution provides the following physical parameters: l_1 =1.505 m, l_3 =0.633 m, l_5 =1.244 m, l_{2Q} =3.382 m, g_2 =0.414 m^{-1}, g_4 =-0.389 m^{-1}.

Using curves shown in Fig.37-40, the absolute deviations of the Twiss parameters can be evaluated for an operating point. Our operating point provides the following relations: $\Delta\beta_{2,x} \approx 0.41 \cdot \Delta\beta_{1,x}$, $\Delta\beta_{2,x} \approx -1.6 \cdot \Delta\alpha_{1,x}$, $\Delta\alpha_{2,x} \approx 0.03 \cdot \Delta\beta_1$, $\Delta\alpha_{2,x} \approx -0.7 \cdot \Delta\alpha_{1,x}$, $\Delta\beta_{2,y} \approx -5.2 \cdot \Delta\beta_{1,y}$, $\Delta\beta_{2,y} \approx -8.3 \cdot \Delta\alpha_{1,y}$, $\Delta\alpha_{2,y} \approx 2.0 \cdot \Delta\beta_{1,y}$, $\Delta\alpha_{2,y} \approx 1.85 \cdot \Delta\alpha_{1,y}$.

Appendix A. Elements of the sensitivity matrix.

$$\frac{\delta_{\beta_2}}{\delta_{\beta_1}} = \frac{\Delta\beta_2/\beta_2}{\underbrace{\Delta\beta_1/\beta_1}_{\delta_{\beta_1}}} = \frac{\overbrace{\left[\beta_2(\beta_1+\Delta\beta_1,\alpha_1)-\beta_2(\beta_1,\alpha_1)\right]}^{\Delta\beta_2}/\beta_2}{\delta_{\beta_1}} = \frac{\beta_2(\beta_1+\Delta\beta_1,\alpha_1)-\beta_2(\beta_1,\alpha_1)}{\beta_2\cdot\delta_{\beta_1}}$$

$$\frac{\delta_{\beta_2}}{\delta_{\alpha_1}} = \frac{\Delta\beta_2/\beta_2}{\underbrace{\Delta\alpha_1/\alpha_1}_{\delta_{\alpha_1}}} = \frac{\overbrace{\left[\beta_2(\beta_1,\alpha_1+\Delta\alpha_1)-\beta_2(\beta_1,\alpha_1)\right]}^{\Delta\beta_2}/\beta_2}{\delta_{\alpha_1}} = \frac{\beta_2(\beta_1,\alpha_1+\Delta\alpha_1)-\beta_2(\beta_1,\alpha_1)}{\beta_2\cdot\delta_{\alpha_1}}$$

$$\frac{\delta_{\alpha_2}}{\delta_{\beta_1}} = \frac{\Delta\alpha_2/\alpha_2}{\underbrace{\Delta\beta_1/\beta_1}_{\delta_{\beta_1}}} = \frac{\overbrace{\left[\alpha_2(\beta_1+\Delta\beta_1,\alpha_1)-\alpha_2(\beta_1,\alpha_1)\right]}^{\Delta\alpha_2}/\alpha_2}{\delta_{\beta_1}} = \frac{\alpha_2(\beta_1+\Delta\beta_1,\alpha_1)-\alpha_2(\beta_1,\alpha_1)}{\alpha_2\cdot\delta_{\beta_1}}$$

$$\frac{\delta_{\alpha_2}}{\delta_{\alpha_1}} = \frac{\Delta\alpha_2/\alpha_2}{\underbrace{\Delta\alpha_1/\alpha_1}_{\delta_{\alpha_1}}} = \frac{\overbrace{\left[\alpha_2(\beta_1,\alpha_1+\Delta\alpha_1)-\alpha_2(\beta_1,\alpha_1)\right]}^{\Delta\alpha_2}/\alpha_2}{\delta_{\alpha_1}} = \frac{\alpha_2(\beta_1,\alpha_1+\Delta\alpha_1)-\alpha_2(\beta_1,\alpha_1)}{\alpha_2\cdot\delta_{\alpha_1}}$$

Let's calculate the absolute deviations of the Twiss parameters for the operating point in the case of MATCH1 for x-plane:

$$\Delta\beta_2 = \frac{\delta_{\beta_2}}{\delta_{\beta_1}}\frac{\beta_2}{\beta_1}\Delta\beta_1 = 0.46\frac{10.84}{6.03}\Delta\beta_1 = 0.8\Delta\beta_1,$$

$$\Delta\beta_2 = \frac{\delta_{\beta_2}}{\delta_{\alpha_1}}\frac{\beta_2}{\alpha_1}\Delta\alpha_1 = 0.45\frac{10.84}{\text{-}1.18} = -4.2\Delta\alpha_1,$$

$$\Delta\alpha_2 = \frac{\delta_{\alpha_2}}{\delta_{\beta_1}}\frac{\alpha_2}{\beta_1}\Delta\beta_1 = 0.095\frac{3.03}{6.03}\Delta\beta_1 = 0.05\Delta\beta_1,$$

$$\Delta\alpha_2 = \frac{\delta_{\alpha_2}}{\delta_{\alpha_1}}\frac{\alpha_2}{\alpha_1}\Delta\alpha_1 = 0.1\frac{3.0}{-1.2}\Delta\alpha_1 = -0.26\cdot\Delta\alpha_1.$$